JOURNAL OF COASTAL AND HYDRAULIC STRUCTURES

Vol. 2, 2022, 19

Investigating Wave Transmission through Curtain Wall Breakwaters under Variable Conditions

Hoang Thai Duong Vu[1], Moritz Zemann [2], Peter Oberle [3], Frank Seidel [4], Franz Nestmann [5]

[1]hoang.vu@kit.edu, Karlsruhe Institute of Technology, 76131, Karlsruhe, Germany
[2]moritz.zemann@kit.edu, Karlsruhe Institute of Technology, 76131, Karlsruhe, Germany
[3]peter.oberle@kit.edu, Karlsruhe Institute of Technology, 76131, Karlsruhe, Germany
[4]frank.seidel@kit.edu, Karlsruhe Institute of Technology, 76131, Karlsruhe, Germany
[5]franz.nestmann@kit.edu, Karlsruhe Institute of Technology, 76131, Karlsruhe, Germany

This paper was submitted on 20 May 2022. It was accepted after double-blind review on 16 August 2022 and published online on 29 September 2022.

DOI: https://doi.org/10.48438/jchs.2022.0019

Cite as: "Vu, H. T. D., Zemann, M., Oberle, P., Seidel, F., & Nestmann, F. Investigating Wave Transmission through Curtain Wall Breakwaters under Variable Conditions. Journal of Coastal and Hydraulic Structures, 2, p. 19. https://doi.org/10.48438/jchs.2022.0019"

Abstract

Coastal erosion has become a pressing problem all over the world, especially in areas where the hinterland is only slightly elevated over the sea level. The ongoing progression reveals the urging need for coastal protection strategies, in which breakwaters are among the possible protection measures. Within the development process of a detached breakwater to face coastal erosion in the Mekong Delta, different concepts of Curtain Wall Breakwater (CWB) configurations have been investigated. Several characteristics of CWB structures such as the inclination with respect to vertical direction, the thickness of the wall, the height of the structures, the rate of submergence and emergence, etc. were examined for different water depths and wave parameters. The wave-structure interaction was analyzed using FLOW3D software, a computational fluid dynamic (CFD) platform based on Finite Volume Method (FVM) to solve the governing equations of fluid motion. Numerical simulations showed a high agreement in wave transmission coefficients with experimental results with the correlation R^2 of 0.89 to 0.93, respectively. Afterwards, wave transmission through different CWB configurations were investigated. The results illustrated a continuous reduction of the wave transmission coefficient with increasing inclination from 90° to 135°, whilst the orientation of the inclination (e.g. 60° vs 120°) only showed a minor effect regarding the wave reduction. All CWB arrangements showed increasing performance with decreasing wave periods. Besides, the wave transmission was mainly impacted by the level of submergence together with the amount of supporting piers and the thickness of the structures. Water depth changes due to tidal influence revealed an increase in wave transmission coefficient once the wave started to overtop the structure.

Keywords

Curtain wall breakwater, transmission coefficient, numerical modeling, physical modeling, Mekong Delta.

1 Introduction

Coastal regions offer versatile cultural and ecosystem services leading to a huge share of the world population living within 100km towards the coast (United Nations 2017). 267 million people live in areas which are located only 2m above the mean sea level with a large proportion of them residing in delta regions such as the Amazon, Ganges-Brahmaputra-Meghna or the Mekong Delta (Hooijer and Vernimmen 2021). This leads to a high vulnerability to seaborne natural disaster and sea level rise, which are mostly connected to the challenges of climate change. Climate change thereby affects the frequency and intensity of storms, increases the global surface temperatures, and sea level rise (Pörtner et al. 2022). As a direct consequence, coastal erosion can be attributed to climate change induced sea level rise (Masselink et al. 2020; Leatherman et al. 2000) and more intense storms leading to an increase in wave energy. Climate change is therefore one of the most serious impacts being faced by coastal systems worldwide.

To reduce or stop land loss driven by coastal erosion, the wave energy needs to be dissipated before reaching the shore. In many tropical and subtropical areas, natural mangrove belts formerly stabilized the coastline, prevented erosion, and protected the land from waves and storms. However, a global loss of mangroves has been reported within the last decades which has been attributed primarily to human activity (Goldberg et al. 2020). Especially areas in Southeast Asia such as Myanmar, Malaysia, Cambodia, and Vietnam are heavily impacted by deforestation (Besset et al. 2019; Hamilton and Casey 2016). Against the background of eroding coasts and the loss of natural protection systems, rapid action is required in many areas, where coastal protection constructions such as breakwater systems, revetments or dykes serve as an engineering measure. However, such structures often imply a massive intervention in the coastal ecosystems and therefore impede a further natural development. As there is often no need for a complete wave energy dissipation, detached solutions with porous breakwater systems would allow hydraulic connectivity and sediment exchange to maintain the ecological connectivity and habitat conditions as well. Curtain wall breakwater types (CWB) have been identified as one possible solution.

While the intentional usage of partially submerged curtain walls is the removal of flotsam from the water surface, they are often used to protect the intake structures of power plants or sewage treatment facilities. However, they also have the potential for dissipation of wave energy (Suh et al. 2006; Rageh and Koraim 2010; Suh et al. 2011; Alsaydalani et al. 2017). Especially in situations, where i) a partial protection of the coast e.g. in terms of wave reduction is needed, ii) the hydraulic connectivity of the protected area needs to be maintained, or iii) the sediment deposition for land reclamation is to be enhanced, they might be of advantage. Due to the slender design of CWB, they are assumed to offer an economically interesting alternative in comparison to massive breakwater constructions (Frese et al. 2012). Besides, due to their pillar-based foundation, their application is considered favorable especially under soft-soil conditions (Franco 1994; Bloxam et al. 2003; Atkins 2019).

Considering the wide range of possible setups and configurations regarding the curtain submergence and emergence, its thickness, and the pile arrangement for foundations, unsurprisingly a lot of different geometric and functional concepts can be found in the literature, namely pile-supported skirt breakwaters/bars (Laju et al. 2011; Koraim 2014), vertical (slotted) wall breakwaters/barriers (Ursell 1947; Isaacson et al. 1998;), wave screen breakwaters (Atkins 2019), submerged (inclined) plates (Parsons and Martin 1992; Yagci et al. 2014; Cho and Kim 2008), or curtainwall(-pile) breakwaters (Subekti et al. 2019; Ajiwibowo 2018; Lee et al. 2009; Zhu et al. 2015; Nejadkazem and Mostafa Gharabaghi 2013; Liu and Li 2011; Suh et al. 2007). All of these refer to a breakwater which is founded on piles featuring a partially submerged and emerged wall, leaving a gap between the seafloor and the lower edge of the wall. In the following, all these concepts are referred to as CWBs.

A main aspect of many studies is the investigation of the wave transmission through the CWB under different hydraulic and geometric conditions (Suh et al. 2007; Subekti and Shulhany 2021; Alsaydalani et al. 2017; Zhu et al. 2015; Ji and Suh 2010). Various studies focused on the effects of breakwater porosity or the blocked share of the cross section e.g. in terms of adding or arranging piers inside the gap below the breakwater wall (Suh et al. 2005, Suh et al 2007, Elsheik et el. 2022) or varying the curtain draft (Koraim et al 2014b, Shao 2005). In general, reducing the hydraulic active cross section thereby leads to a reduced wave transmission (Rageh and Koraim 2010; Subekti et al. 2019). The arrangement and staggering of different numbers of curtains was found to be a relevant factor for the CWB efficiency indicating a stepwise reduction of the wave transmission with increasing number of consecutively arranged curtains (Isaacson et al. 1999; Isaacson et al. 1998). In terms of wave characteristics, the decrease in wave transmission with

increasing wave numbers (kh) was observed (Isaacson et al. 1998; Liu and Li 2011; Ajiwibowo 2018; Alsaydalani et al. 2017). Besides, a better performance of CWB was seen in the context of steep waves (Subekti and Shulhany 2021; Subekti et al. 2019; Ajiwibowo 2018; Elsheikh et al. 2022). In addition, some research was also done regarding inclined curtain walls, Yagci et al. (2014); Acanal et al. (2013) investigated inclined curtain walls for shallow inclined plated 0° to 15°. Within the experiments, the inclination between 0° to 15° did not reveal a significant impact to the transmission coefficient, however best wave attenuation could be attributed to the combination of the largest inclination with the largest submergence. Besides, Rao et al. (2009) performed experiments on changing inclined plate breakwaters under fully submerged conditions. They found the inclination of 60° to act most effective for the entire range of applied wave parameters while the orientation of the inclinations seemed of minor relevance.

The mentioned studies above show a good potential of CWBs in wave damping capacity, only limited information of CWBs in practical applications is available. One example has been reported from Malaysia, where the ferry terminal of Tawau was protected by a partial depth wave screen. The CWB there was chosen based on the need for a detached installation under soft soil conditions, and a wave height reduction of 50% was considered sufficient to protect the behind ferry port (Atkins 2019). Another CWB was constructed to protect the marina of Laboe (Germany). As ship-induced waves were not damped sufficiently by the CWB which was originally dimensioned for the wind waves, as a countermeasure, the bottom gap was later closed by sheet pile walls (Frese et al. 2012). The protection of the Raffles Marina in Singapore was realized by installing a vertical slotted wave screen. Due to the soft seabed, a pile foundation was favored here against conventional breakwater types (Bloxam et al. 2003). A vertical breakwater was installed in the early 70s at Manfredonia port (Italy) to protect the harbor. The pillar-based installation with a curtain over the water depth was mainly driven by soft soil conditions (Franco 1994).

All cited theoretical and experimental studies in this section already feature a wide range of results and therefore provide a good database for further considerations of the CWB as a potential coastal protection measure. However, their results are often limited to their specific investigated conditions and can not easily be transferred as a general approach to a specific study area, e.g. the Mekong Delta (MD). Especially, the effects of overtopping under tidal variations and the evaluation of inclined walls compared to a vertial wall are not comprehensively investigated.

The main aim of this study is to investigate wave transmission through different CWB geometries under various hydraulic conditions relevant for the MD and similar coasts. After validation of the numerical approach with physical modeling results, the wave-structure interaction was systematically examined in numerical platform including the effects of the curtain inclination, the thickness of the wall, the supporting piers, the submergence rate, and the influence of wave overtopping for different tidal ranges are considered. This study comprehensively demonstrates the influence of CWB configurations on the wave damping efficiency and therefore provides additional findings to this subject area.

2 An overview of the coastal protection works in the Mekong Delta

Being one of the most important areas for agricultural and aquaculture production of Vietnam and for the world market (Vu et al. 2022; Nguyen et al. 2022), the MD has been increasingly affected by coastal erosion and land subsidence (Minderhoud et al. 2018; Kim et al. 2021) within the last decade as a result of sediment misbalance and groundwater over-abstraction (Anthony et al. 2015). Besides, it has faced serious challenges in the recent years due to flooding (Tran et al. 2021; Vu et al. 2016; Vu 2019), drought (Nguyen et al. 2021), salinity intrusion (Park et al. 2021), and the impact of hydropower dams on the upstream Mekong River (Hecht et al. 2019). The development of hydropower dams has reduced discharge and discharge variations (Dung et al. 2021) and sediment transport from the upstream Mekong River into the sea decreases dramatically (Le et al. 2019). Furthermore, large-scale sand mining along the main rivers of the MD has caused morphological changes and riverbank erosion in recent years (Jordan et al. 2019; Gruel et al. 2021). Climate change induced sea level rise adds some additional pressure on the MD (Minderhoud et al. 2019) due to its low elevation ranging mostly below 2.0 m a.m.s.l (Vu et al. 2014). As a result, coastal erosion and mangrove belt degradation have occurred severely along the coastal strip (Le et al. 2021). While mangroves feature an important role in the natural protection of the coastline (Marchesiello et al. 2019; Besset et al. 2019), it becomes obvious that the ongoing mangrove squeeze (Phan et al. 2015) leads to an urgent demand for engineering solutions such as breakwaters.

A range of hard and soft measures (Figure A1 in the Appendix) have been built along the coastline of the MD to prevent coastal erosion and enable mangrove restoration (Minh et al. 2020; Albers and Stolzenwald 2014; Albers et al. 2013). Several hard measures, i.e., porous breakwaters, pile-rock breakwaters, and semi-circular ones, have been built within the last decade (Le et al. 2020; Luom et al. 2021). Some of them seem to work effectively in wave damping and enrich sediment deposition, nevertheless, others failed due to the soft soil condition and missing foundation concepts (DARD Camau 2021). In addition, the construction of the hard structures requests a huge amount of building materials which are not available in the region. Soft measures with low construction costs and simple installation such as bamboo and melaleuca fences or geo-tube breakwaters have also been tested in the MD (Dao et al. 2021; Tuan and Luan 2020; Chu et al. 2015; Albers and Stolzenwald 2014). However, the bamboo fences have a short lifespan of only 1–2 years under wave conditions (Le et al. 2021), while the geo-tube breakwaters are vulnerable to sharp shells and physical collisions that might cause damage or deformation (Nugroho et al. 2021; Shin et al. 2019). Figure 1 illustrates some failure examples of breakwaters in the MD including a soft measure (T-fence bamboo) and hard measures (pile concrete wall, vertical and horizontal hollow breakwaters).

Figure 1: Some failure examples of breakwater in the MD (Source: images were provided by Ca Mau DARD).

Our study was conducted within the framework of the ViWaT Engineering project sponsored by the Federal Ministry of Education and Research (BMBF, Germany), which overall intends to develop an innovative breakwater concept to counteract the coastal erosion in the MD (Figure 2). In this context, considering the relevant onsite aspects e.g. the local wave heights, tidal variations, soft soil condition, etc., piers-based concepts like a CWB might become a suitable solution in terms of stability and minor demand of construction materials for the eroding coastline there.

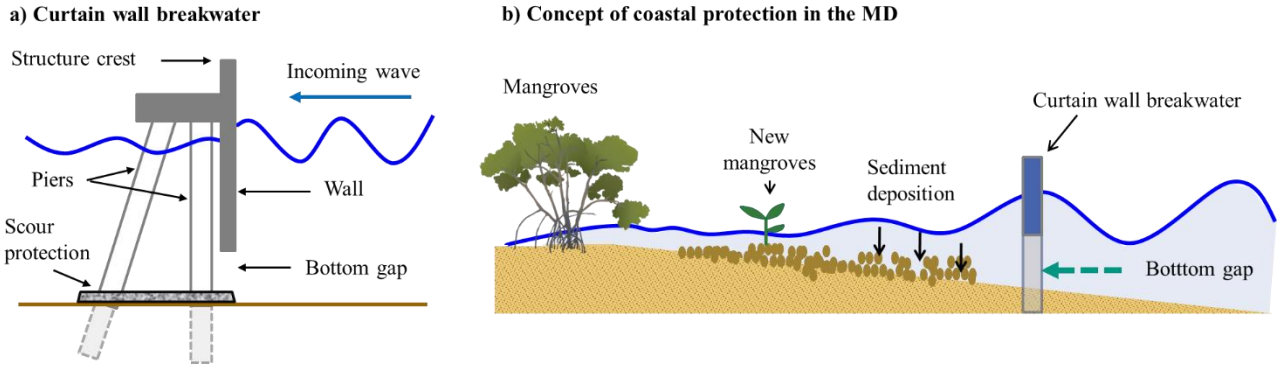

Figure 2: a) Generalized concept of a curtain wall breakwater; b) Concept of breakwater implementation, sediment deposition, and mangrove replantation for the MD.

3 Methodology

3.1 Wave-structure interaction

The wave interaction with breakwaters can be generally described by three factors, i.e., the wave transmission coefficient (K_t), the reflection coefficient (K_r), and the dissipation coefficient (K_d).

The transmission coefficient (K_t) is the most dominant indicator to assess the effectiveness of breakwaters. It enables to calculate the wave characteristics behind the structures and therefore is used to evaluate the performance of breakwaters. Waves hitting a structure are partly reflected, which leads to an interaction of the incident and reflected waves on the seaside of the structure. The reflection coefficient (K_r) is used to define the reflected wave with respect to the incident wave. The dissipation coefficient (K_d) is used to describe the proportion of wave energy dissipated by the breakwater. This cannot be measured and instead is a derived value based on the transmission and reflection coefficients. Refering to Le et al. (2021); Dao et al. (2021), the dissipation coefficient (K_d) can be calculated following Equation 1:

$$K_t^2 + K_r^2 + K_d^2 = 1 \quad (1)$$

where the transmission and reflection coefficients are defined as:

$$K_t = \frac{H_t}{H_i} \quad (2)$$

$$K_r = \frac{H_r}{H_i} \quad (3)$$

and H_i, H_r, H_t correspond to the incident, reflected, and transmitted wave heights.

In this study, WaveLab software developed by Aalborg University, Denmark (Aau, 2022) was used to analyse the wave parameters of physical and numerical tests.

3.2 Physical modeling

A wave flume at the Theodor-Rehbock Laboratory (TRL) of the Institute for Water and River Basin Management at Karlsruhe Institute of Technology (KIT-IWG) was used to perform the experiments for validation of the results from the numerical study. The wave flume is 22 m in length (effective length), 0.6 m in width, and 0.6 m in height. The flume was manufactured with glasses on the sides and a smooth concrete surface at the bottom with the Manning's roughness coefficient of 0.01 to 0.013, respectively to minimize the friction and roughness of the sides and flume bed. Wave absorbing layers are installed to minimize reflection from both ends of the flume. Absorbing layers are sharp-edged and smooth stones / rocks with different sizes (0.2 cm, 0.5 cm, 1 cm, 2 cm, 3cm, 5cm) that were filled homogeniously on an inclined and metal sheet with holes of 0.1cm. Tap water was used for the tests with a density of 1000 m^3/kg. Experiments were performed in sommer time, therefore, the room temperature varied from 25 to 30 °C, while the water temperature varied from 20 to 25 °C.

Waves are generated by a wave paddle which consists of a trapezoidal corpus, featuring a backlog inclination towards the flume to press the waves into the flume. The paddle is operated regularly up and down by a hydraulic lever arm. The speed can be controlled by adapting the pressure into the hydraulic system. The diving depth can be controlled by changing the distance of the lever arm. Due to this mechanism, the wave generator can operate only regular waves in terms of wave heights and wave periods in a certain range. However, it cannot generate random waves to simulate the energy spectrum models to represent the sea waves.

Figure 3 shows the experimental setup in the TRL laboratory, KIT-IWG, whereas Figure 4 shows the position of the wave sensors and the general layout of the experiment. Particularly, four capacitive wave gauges were installed in the middle of the flume to measure wave signals at a sampling frequency of up to 20 Hz. Three wave gauges (WG1, WG2, WG3) in front of the structure were installed following the method by Masard and Funke (1980) to detect the incident and reflection wave heights, while WG4 is located behind the breakwater to measure the transmitted wave height. WG1 and WG4 have a unique distance of a wave length (λ) to the structure. The probe spacings between WG1 to WG2 and WG3 are installed following the approach introduced by Masard and Funke (1980) as:

$$X1a = \lambda/10$$

$$\lambda/6 < X1b < \lambda/3 \quad \text{and} \quad X1b \neq \lambda/5 \quad \text{and} \quad X1b \neq 3\lambda/10$$

The scale of the physical model was selected of 1:10 based on the ability of the wave flume to house the breakwater and the input wave boundary conditions. The physical model was set up following Froude's law to ensure the similarity

of hydrodynamic conditions. Froude number expresses the ratio between gravity and inertia forces within the hydrodynamic system as written in Equation (4).

$$Fr = \frac{v}{\sqrt{gL}} \tag{4}$$

where Fr is Froude number (-), v is flow velocity (m/s), g is gravitational acceleration (m/s^2), and L is length characteristics. The model scale is deduced according to the Froude similitude as follows: $N_L = \frac{L_{prototype}}{L_{model}} = 10$ (geometric scale), $N_t = \sqrt{N_L} = \sqrt{10} = 3.16$ (scale of time), $N_v = \sqrt{N_L} = \sqrt{10} = 3.16$ (scale of velocity), and $N_m = N_L^3 = 10^3 = 1000$ (scale of mass).

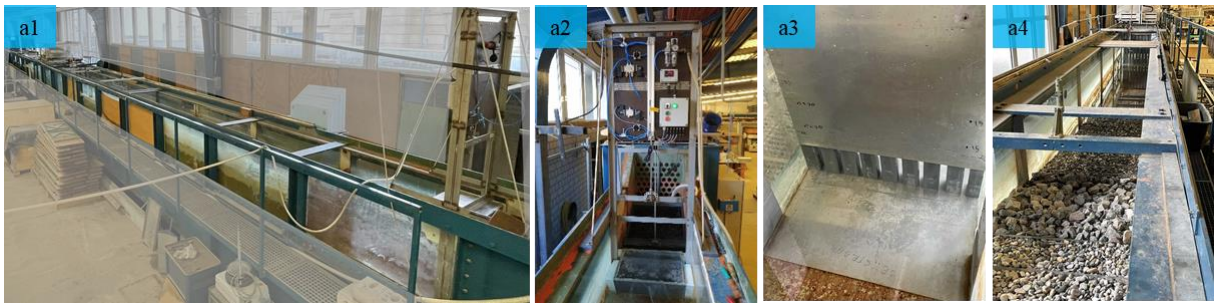

Figure 3: General view of the wave flume (a1); Wave paddle and control unit (a2); CWB structure with eight supporting piers (a3); Wave absorbing layer (a4).

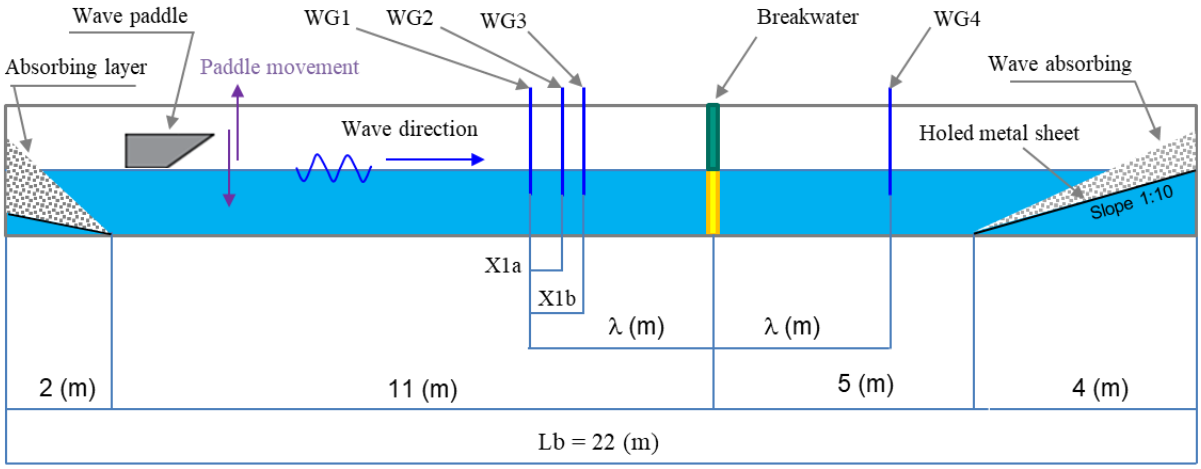

Figure 4: Sketch of wave flume arrangement in the laboratory.

3.3 Numerical modeling

FLOW3D is a commercial computational fluid dynamics (CFD) software developed by Flow Science Inc. This code uses of Finite Volume Method (FVM) to solve governing equations of fluid motion (Fuentes-Perez et al. 2022; Bayon et al. 2016). Several turbulence modeling options are integrated in numerical schemes for simulating turbulent flows. These include Prandtl's mixing length theory, one-equation turbulent energy (k), two-equation turbulent energy (k-ε), Renormalized Group (RNG), and Large Eddy Simulation (LES) models. Besides, this CFD platform uses an orthogonal coordinate system as opposed to a body-fitted system and can have a single nested mesh block, adjacent linked mesh blocks, or a combination of nested and linked mesh blocks (Flow Science 2008).

FLOW3D has been applied to numerous research fields such as hydraulic structure design (Musall and Oberle 2014; Fuentes-Pérez et al. 2022; Song and Vu 2012), weir and dam analysis (Hu et al. 2018), scour processing (Behnam et al. 2016), sediment transport (Kosaj et al. 2022), flow resistance of vegetation (Abdurrasheed et al. 2019; Fard 2020), and flood management (Gems et al. 2016). Besides, this CFD platform simulates regular linear and nonlinear waves (Stokes,

Stockes and Cnoidal, and Solitary) as well as random waves. A linear wave has a sinusoidal surface profile and generated using Airy's linear wave theory. The elevation of a linear component wave is expressed as

$$\eta = A\sin(\omega t+\varphi) \quad (5)$$

where A, ω, and φ are wave amplitude, angular frequency and initial phase, respectively (Flow Science 2008). While irregular waves can be defined by either using multiple sinusoidal linear component waves with independent frequencies, amplitudes and initial phases, or using random wave generator based on a wave energy spectrum, i.e., JONSWAP or Pierson-Moskowitz.

In this study, two wave flumes were used in the CFD platform. First, a model was set up with the same dimensions as the small-scale physical model (1:10) shown in Figure 4 to examine the agreement of the numerical approach with experimental tests. Then, a second model was applied to investigate further the wave interaction against CWB configurations at the full-scale (1:1) to be more convenient to transfer the concept to the field under wave conditions in the MD.

The settings in the numerical models are briefly described, e.g., the computational domain is covered with hexahedral cells; liquid properties include water at 20 °C, density of 1,000 kg/m^3, dynamic viscosity of 0.001 kg/m/s; time-step is controlled by "Stability and convergence" and automatically adapted in order to ensure that Courant–Friedrichs–Lewy (CFL) numbers remain below a threshold of 0.45; advection is discretized using a second order scheme while the fluid fraction is solved with the default Volume of Fluid (VOF) scheme (Hirt and Nichols 1981).

Figure 5 shows the wave flume with the arrangement of wave gauges and structures on the full-scale numerical platform. The wave gauges (WG1, WG2, WG3) were arranged following the method by Masard and Funke (1980). Here, WG1 and WG4 were placed in front of and behind the structure with the same distance of a wave length (λ), while the breakwater was located three wave lengths from the inlet (WG0) to minimize the effect of the reflection caused by the breakwater that may pollute the incoming wave as FLOW3D does not have a "relaxation zone" (REEF3D, 2022) to absorb the reflection wave caused by the breakwaters. The wave-absorbing layer was set up at the end of the wave flume to absorb the residual wave energy. The distance X from WG4 to the absorbing layer was arranged as a wave length for short-wave periods of 2 s to 3.5s, whilst X of 3 m for long-wave periods of 4s to 8s to save the computational time and to ensure the absorbing layer do not cause any effect to the WG4. The total length of the wave flume (Lb), therefore, is approximately five to six times the wave length.

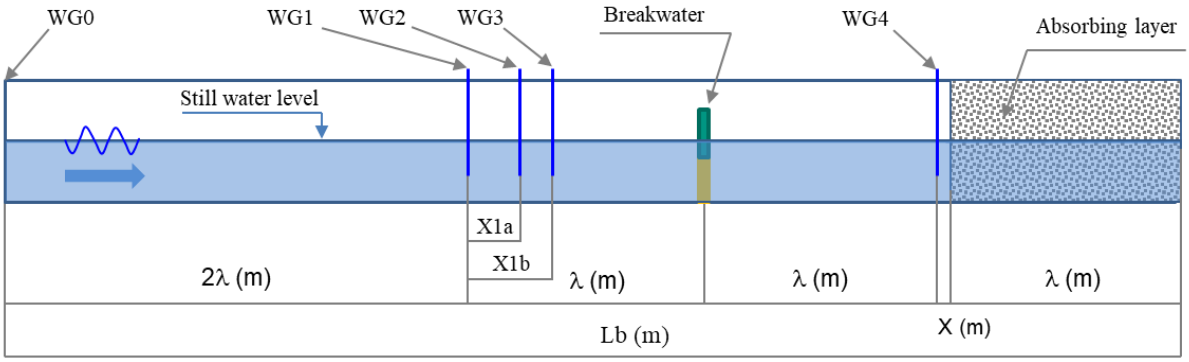

Figure 5: Sketch of the wave flume in the numerical model to simulate the full-scale waves in the MD.

3.4 Wave boundary conditions

Based on investigations and surveys of the nearshore wave conditions in the MD, the average significant wave height at the nearshore ranges from 0.5 m to 0.85 m, and the average wave periods vary from 3.5 – 4.2 s on the West coast and 4.4 - 5.5 s on the East coast (Minh et al. 2020). The boundary conditions used in our experiments are presented in Table 1. First, we investigated the wave interaction against the CWB for a broader range of relevant periods of 2 s up to 8 s. Afterwards, the wave period of 4s was selected as the most dominant one in the region to study more comprehensively with different wave heights and water depths. Specifically, the water depth ranges from shallow water at 2 m to deep water at 5 m, while the wave heights vary from 0.2 m to 1.0 m.

Table 1: Boundary conditions for testing the wave damping against CWBs.

No.	Water depth h (m)	Wave height Hs (m)	Wave period Tp (s)	Wave	Approach
1	2.0	0.2; 0.4; 0.5	4.0	Regular	CFD
2	3.0	0.2; 0.4; 0.6	4.0	Regular	CFD
3	4.0	0.2; 0.4; 0.6; 0.8; 1.0	2.0; 3.0; 3.5; 4.0; 5,0; 6.0; 8.0	Regular	CFD
4	5.0	0.2; 0.6; 1.0	4.0	Regular	CFD

For validation of the CFD platform, two regular waves were examined in the laboratory at the KIT-IWG in the scale of 1:10. Additionally, we performed further 15 tests in numerical modeling to validate with physical results from literature, i.e., by Suh et al. (2005). The wave characteristics for validation of CFD platform were shown in Table 2.

Table 2: Boundary conditions for validation of numerical model based on laboratory experiments.

No.	Water depth h (m)	Wave height Hs (m)	Wave period Tp (s)	Wave	Approach	Scaled physical model
1	0.2	0.05; 0.1	0.8; 1.4	Regular	CFD & Experiment (KIT-IWG)	1:10
2	2.4	0.1; 0.2; 0.3; 0.4; 0.5	1.5; 2.0; 2.5; 3.0; 4.0	Regular	CFD & Experiment (Suh et al. 2005)	1:1

3.5 Geometric configurations of Curtain Wall Breakwaters (CWBs)

We investigated the wave interaction with different CWB configurations in terms of wave heights and wave periods, the effect of overtopping (structural height), water depth, supporting piers, the gap spacing between the piers, the thickness of the wall, and the inclination of the structure. Table 3 provides the list of CWB configurations that were examined, in which the first seven structures (Nr. 1 to 7) were tested to validate the reliability of numerical approach with the small-scale and full-scale experiments, while the remaining 25 structures (Nr. 8 to 32) were used to investigate the wave transmission through the CWBs in the numerical approach in full-scale of the wave characteristics in the MD. Figure 6 illustrates the schematic of CWBs with different inclinations and supporting piers.

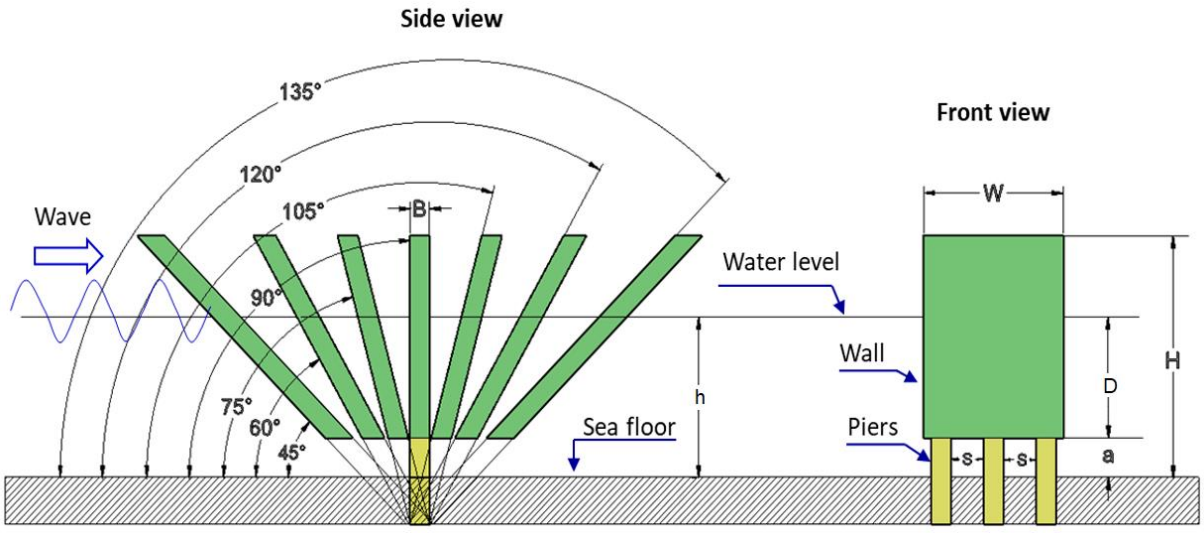

Figure 6: Sketch of different geometrical CWB configurations.

Where H corresponds to the structural height, *W* is the flume width, *B* is the thickness of the wall, *a* is the bottom gap, *S* corresponds to the distance between the supporting piers, α is the inclination of the structure, D is the draft of the wall (submerged depth of the wall from the still water level), and *h* is the water depth, respectively.

Table 3: List of geometrical CWB configurations.

No.	Name	Structure height H (m)	Width B (m)	Bottom gap A (m)	Number of piers	Spacing distance S (m)	Inclination I (°)	Scale	Purpose
1	A0.1S0.2	0.4	0.05	0.1	3	0.2	90	1:10	
2	A0.2S0.2	0.4	0.05	0.2	3	0.2	90	1:10	Model validation
3	A0.1S0.02	0.4	0.05	0.1	8	0.02	90	1:10	(KIT-IWG)
4	A0.2S0.02	0.4	0.05	0.2	8	0.02	90	1:10	
5	D1.44	3.5	0.143	0.96	3	0.143	90	1:1	Model validation
6	D0.96	3.5	0.143	1.44	3	0.143	90	1:1	(Suh et al. 2005)
7	D0.48	3.5	0.143	1.92	3	0.143	90	1:1	
8	I_45°	6	0.5	1	0	-	45	1:1	
9	I_60°	6	0.5	1	0	-	60	1:1	
10	I_75°	6	0.5	1	0	-	75	1:1	
11	I_90°	6	0.5	1	0	-	90	1:1	Effect of inclination
12	I_105°	6	0.5	1	0	-	105	1:1	
13	I_120°	6	0.5	1	0	-	120	1:1	
14	I_135°	6	0.5	1	0	-	135	1:1	
15	B0.05	6	0.05	1	0	-	90	1:1	
16	B0. 5	6	0.5	1	0	-	90	1:1	
17	B1.0	6	1.0	1	0	-	90	1:1	Effect of thickness
18	B2.0	6	2.0	1	0	-	90	1:1	
19	B3.0	6	3.0	1	0	-	90	1:1	
20	D1.0	Non-overtopping	0.5	Follow water depth	0	-	90	1:1	Effect of submerged draft and water depth
21	A1S-	6	0.5	1	0	-	90	1:1	
22	A2S-	6	0.5	2	0	-	90	1:1	
23	A3S-	6	0.5	3	0	-	90	1:1	Effects of piers and
24	A1S0.2	6	0.5	1	4	0.2	90	1:1	bottom gaps
25	A2S0.2	6	0.5	2	4	0.2	90	1:1	
26	A3S0.2	6	0.5	3	4	0.2	90	1:1	
27	H4S-	4	0.5	1	0	-	90	1:1	
28	H4S0.2	4	0.5	1	4	0.2	90	1:1	Effects of structural
29	H6S-	6	0.5	1	0	-	90	1:1	heights and piers
30	H6S0.2	6	0.5	1	4	0.2	90	1:1	
31	H4S0.2	4	0.5	1	4	0.2	90	1:1	Effects of water depth
32	H6S0.2	6	0.5	1	4	0.2	90	1:1	and structural heights

4 Results and discussions

This chapter describes the CFD platform verification (Section 4.1) based on the small-scale physical results (Sub. 4.1.1). Then, the sensitivity analysis of wave transferring along the flume (with and without the structure) and the validation with full-scale experiments in the numerical code is presented (Sub. 4.1.2). Afterwards, the results of the numerical simulations are described to examine the effect of CWB configurations (Section 4.2) including the variations of the wall inclination (Sub. 4.2.1), the effect of structural thickness (Sub. 4.2.2), the effect of submerged draft and water depth (Sub. 4.2.3), the supporting piers and the bottom gaps (Sub. 4.2.4), the influence of wave overtopping and non-overtopping (Sub. 4.2.5), and the effect of structure height and water depth (Sub. 4.2.6).

As the wave transmission coefficient (K_t) is the most relevant factor for evaluating the breakwater efficiency, the data analysis within this study is mainly focused on the K_t. In addition, the wave reflection (K_r) and wave energy dissipation (K_d) were analyzed for the inclined scenarios, as not much research has been done so far to investigate the effect of inclined CWB configurations.

4.1 Numerical model verification

4.1.1. Small-scale laboratory model (1:10)

In a first investigation step, the numerical code was verified based on the experimental results of the scaled physical model (1:10). A sensitivity analysis of several input parameters in the numerical model was performed. The adjusted parameters in the numerical model included bed roughness Ks (0m; 0.002m; 0.005m), grid sizes (0.02m; 0.01m; 0.005m), and different types of regular waves (Linear, Stokes, Stokes and Cnoidal). The simulation time was set up for 40 seconds, the breakwater A0.1S0.02 was examined. Based on the calibration results (see Figure A2 in the Appendix), the parameters of the small-scale numerical model were chosen with a grid size of 0.005 m, roughness K_s = 0 m for linear waves.

The numerical model was further validated with other CWB configurations including A0.2S0.02, A0.1S0.2, A0.2S0.2 with different submerged rates and pier spacings, as pier-spacing and bottom gaps act most significantly on the wave breaking efficiency of the structures (Suh et al. 2005; Subekti et al. 2019), therefore, we selected these configurations to test during the experiments (Figure 7a). Two boundary conditions of short and long wave periods were conducted in both numerical and physical models. The emergence of the CWBs reached the top of the model to avoid overtopping. Generally, eight tests were performed in both numerical and physical models. Figure 7b displays a high agreement regarding the transmission coefficients though the CWB configurations were plotted versus the relative wave number (kh) between numerical simulations (circles) and experimental tests (crosses). Here, the three structures A0.1S0.02, A0.2S0.02, A0.1S0.2 demonstrated in blue, green, and orange colors display high agreement between numerical and physical models. Only the variant CWB A0.2S0.2 shows less accordance with a difference of 7 % - 18% in wave transmission rate between numerical (black circles) and physical models (black crosses), the K_t varies from 0.78 to 0.95.

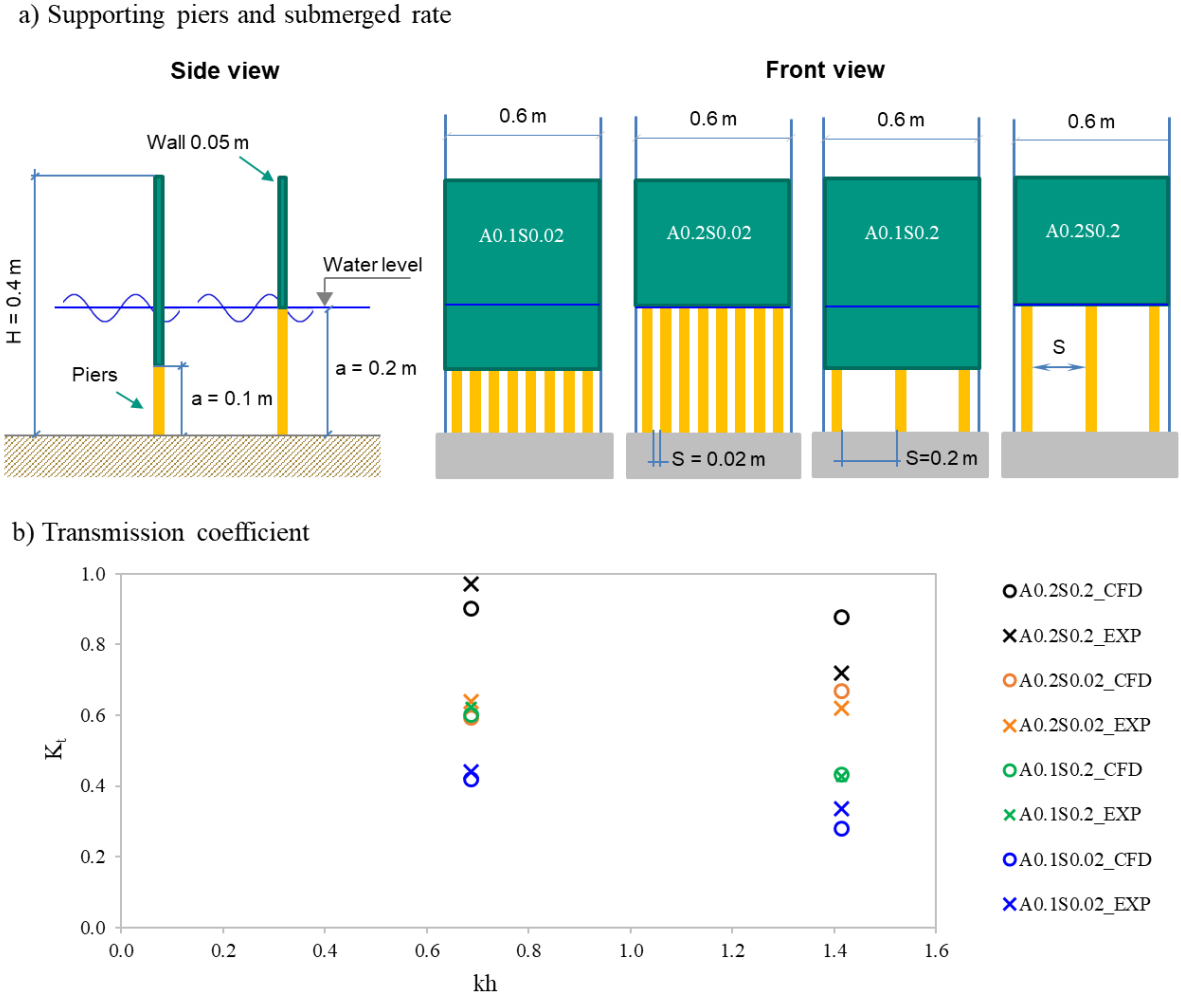

Figure 7: Agreement of wave transmission coefficients between numerical simulations (CFD) and scaled experiment tests (EXP) at the KIT-IWG.

4.1.2. Full-scale model for Mekong waves

First, a sensitivity analysis in the full-scale model for Mekong waves was performed to examine the wave transformation along a blank flume in the numerical approach. Adjusted parameters for this process included surface roughness, turbulence options, grid sizes, and different types of regular waves. The simulation time was chosen to be 100 seconds. The input parameters including a wave height of 0.4 m, wave period of 4 s, and water depth of 2 m were tested. According to Brekke et al. 2005, the waves should be of near permanent form and the height of the waves from one cycle to the next within the examined duration should have minimum prescribed fluctuations for an acceptable regular wave. Therefore, we analyzed the waves in the most stable interval of around 10 waves from 45s to 85s, see Table A1 and Figure A3 in the Appendix. Hence, the inputs with grid sizes of 0.05 m, Large Eddy Simulation (LES) model; Ks = 0 m (surface roughness is neglected), and linear wave could ensure the wave transferring to be maintained along the whole flume.

a) A section of wave flume with the structure I_120 °, water depth of 4 m

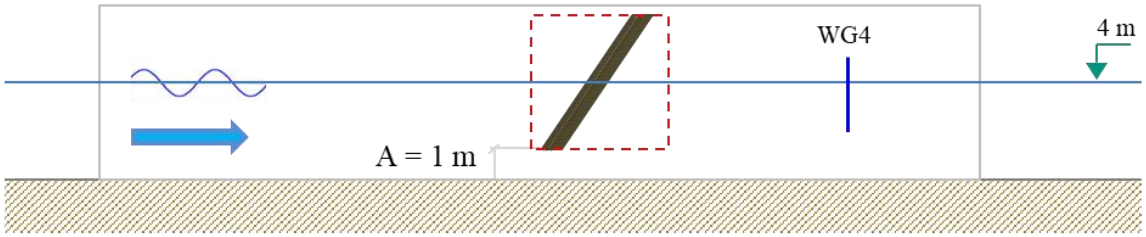

b) Grid size options for the structure I_120°

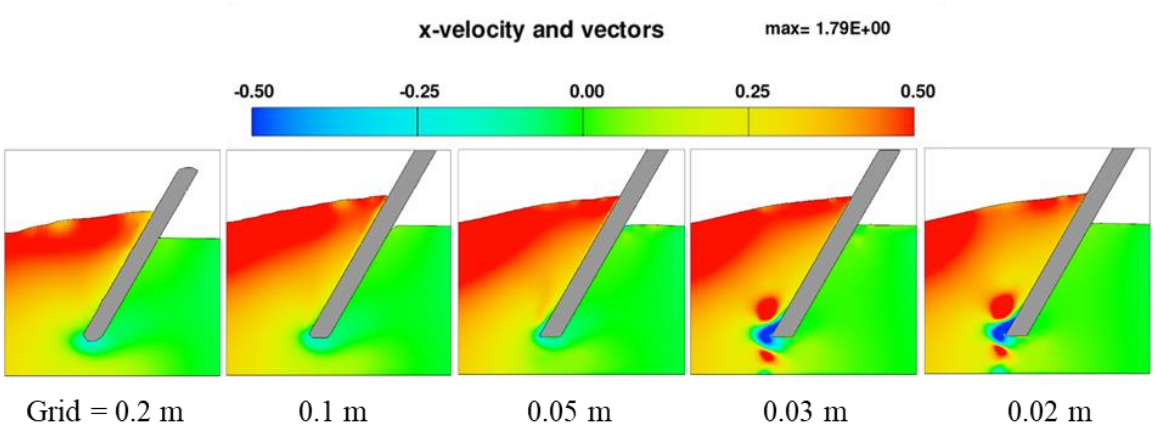

c) Wave transmission coefficient through the structure I_120°

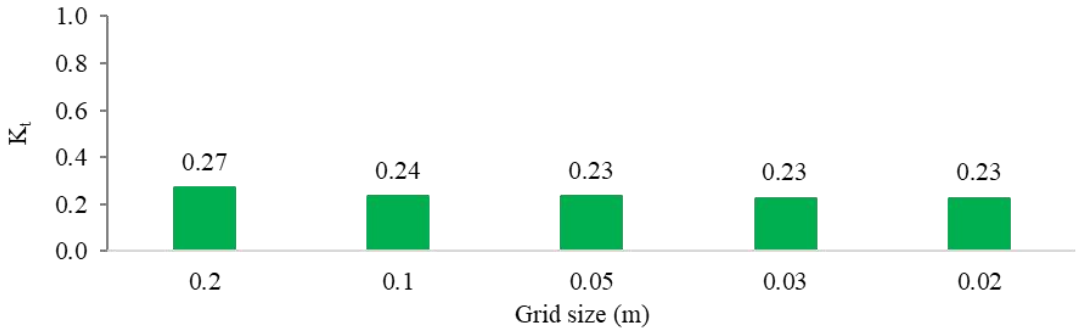

Figure 8: Sensitivity analysis of grid sizes simulated in FLOW3D with the structure I_120°.

Second, a sensitivity analysis of grid sizes for the structure I_ 120° placed in the flume with a bottom gap of 1m was performed. Grid size options range from coarse (0.2 m) to very fine (0.02 m), see Figure 8a. The input parameters include surface roughness (K_s = 0 m), LES model, and linear wave with a water depth of 4 m, wave height of 0.6 m, and wave

period of 4 s. It can be seen that the velocity distributions are better illustrated in finer grid sizes from 0.2 m to 0.02 m as seen in Figure 8b. The structure I_120° can basically be simulated in its full shape with the grid size of 0.05m with the wave transmission coefficient K_t = 0.23 (Figure 8c). In contrast, the model can partly capture the shape of the structure in the coarse grid sizes of 0.2 m and 0.1 m with the K_t values of 0.27 and 0.24, respectively. Besides, finer grid sizes of 0.03 m and 0.02 m can completely simulate the edges of the structure and produce a K_t value of 0.23. However, this leads to a very high demand of computational performance, long simulation time, and big data storage while the differences in K_t values are insignificant. Therefore, we selected the parameters for the full-scale model of grid-size (0.05 m), LES model, the surface roughness (K_s = 0 m), and linear wave as an appropriate setup.

To increase the reliability of the numerical approach, a validation with experimental results by Suh et al. (2005) was additional performed. Specifically, three configurations of D1.44, D0.96, and D0.48 were examined in numerical modeling as shown in Figure 9a. The structures have the same heights, constant pier spacing and thickness with different submerged rates. Figure 9b presents the comparison of K_t values between numerical simulations (CFD, circles) and physical tests (EXP, rectangulars) plotted against the relative wave number (kh). It can be seen that, the results from CFD simulations show a high agreement with EXP results for all three cases of D/h = 0.2 (green), 0.4 (blue), 0.6 (orange). Only a large difference for the case of D/h = 0.2 was noticed at the kh = 2.5, where the CFD values show significantly higher than CFD values, see dashed black circle in Figure 9b.

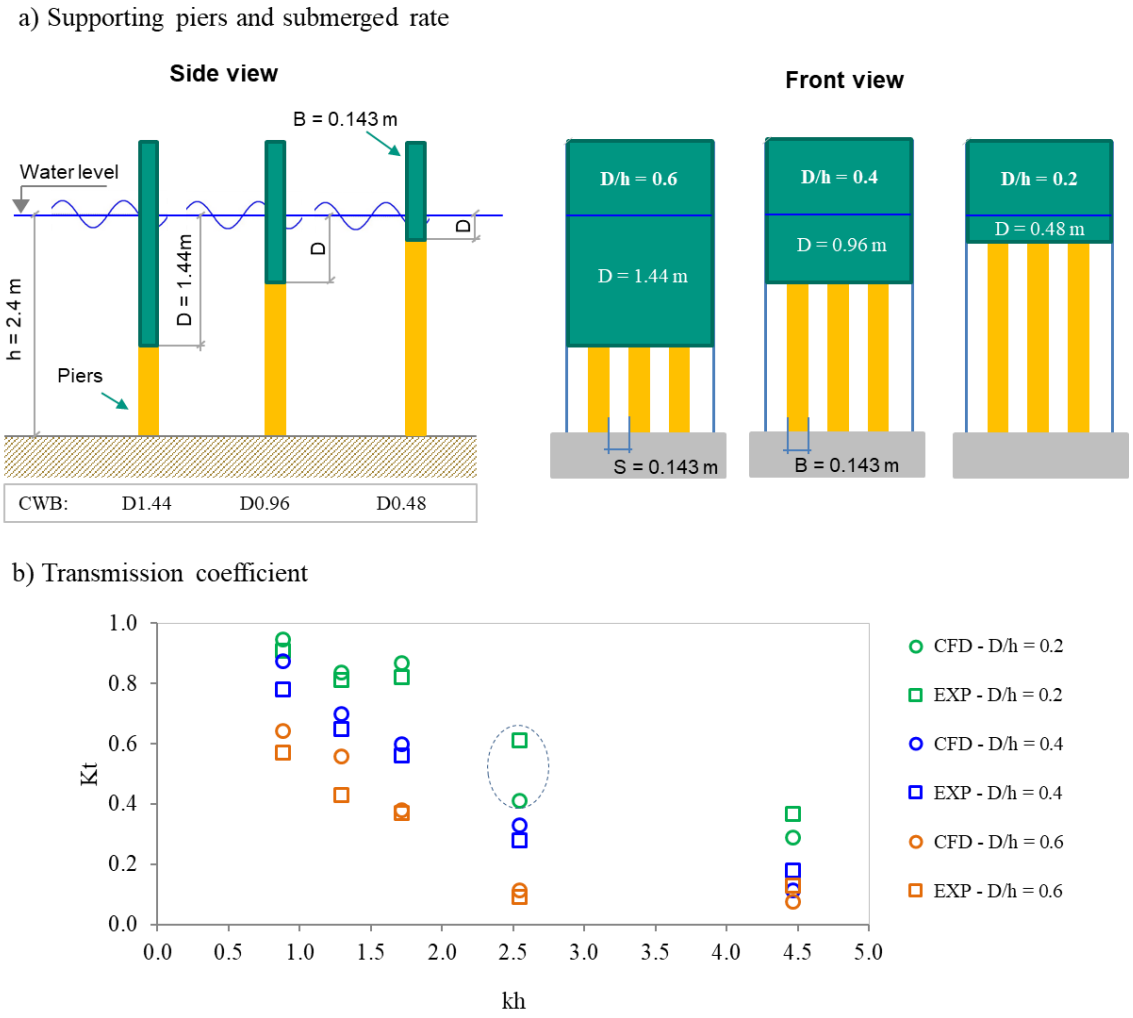

Figure 9: Comparison of wave transmission coefficients (Kt) between numerical simulations (CFD) and experiment results (EXP) by Suh et al. (2005)

Overall, a high agreement of wave transmission coefficients (K_t) between simulation results with physical tests was presented in Figure 10 with the correlation R^2 = 0.89 to 0.93 in the scales of 1:10 (Sub-section 4.1.1) and 1:1, respectively. We considered that FLOW3D is reliable for further investigations of wave-structure interactions in the next section.

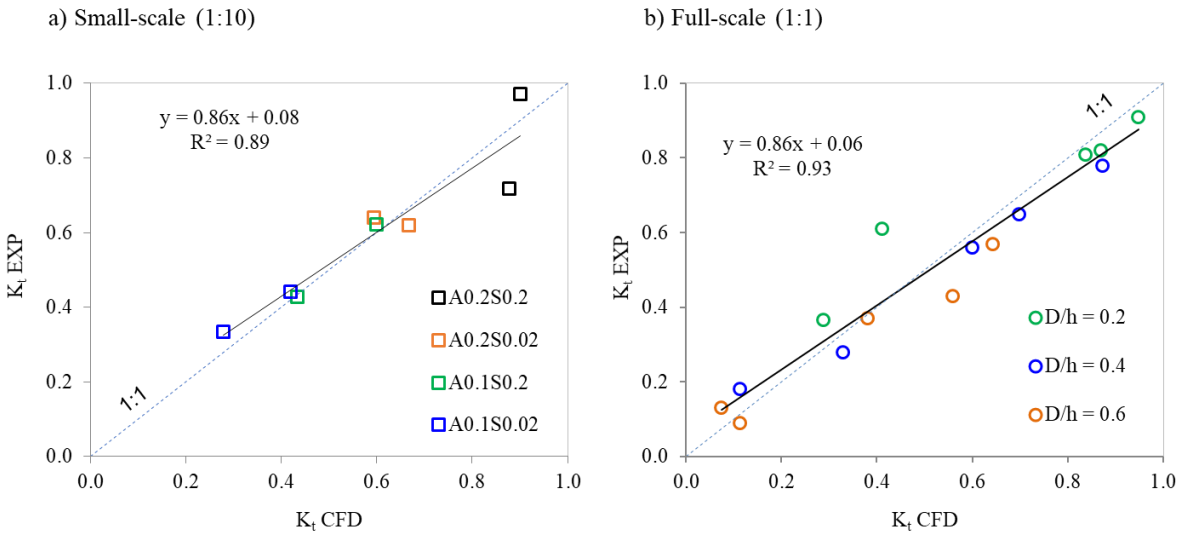

Figure 10: Correlation of K_t values between numerical (CFD) and experimental results (EXP) in small-scale (a) and full-scale (b).

4.2 Investigations on the effects of different CWB configurations

4.2.1. Effect of the wall inclination

A comprehensive investigation on the impact of inclined walls was performed for eight CWBs with different angles of 45°, 60°, 75°, 90°, 105°, 120°, and 135°, respectively. These CWB configurations feature the same thicknesses of 0.5m and heights of 6m, a constant submergence leaving a bottom gap of 1m, without further supporting piers, see Figure 11a. The range of wave periods of 2 s, 3 s, 3.5 s, 4 s, 5 s, 6.5 s, and 8 s were simulated corresponding to the wave heights of 0.6 m and 1 m, respectively in the water depth of 4 m.

Figure 11b shows the results of the wave transmission coefficient (K_t) plotted versus the relative wave number (kh), power trendlines are applied to illustrate the trend. It can be seen that a clear trend of wave transmission reduction is given from 90° towards the angles of 135° or 45°, while there are no relevant differences between positive and negative orientations. Same angles in opposite orientations, i.e., 45° vs 135°, 60° vs 120°, and 75° vs 105° show relatively similar wave transmission coefficients. In addition, the higher the relative wave number, the smaller the transmission coefficient. This means that short wave periods have a better wave damping efficiency than longer ones for all inclinations of CWB configurations.

The reflection coefficients (K_r) of the CWB variants from 90° to 135° were examined based on logarithmic trendlines as shown in Figure 11c. The wave reflection indicates an opposite trend with the transmission coefficient. The structure I_135° causes the highest reflection, followed by the I_120°, I_105°, while the I_90° shows the lowest reflection.

The energy dissipation coefficients (K_d) are plotted versus the wave number (kh), and the linear trendlines are used as shown in Figure 11d. A relatively similar wave damping efficiency of all investigated inclinations is illustrated. It is interesting to recognize that the I_90° performs almost in the same way in wave energy dissipation in comparison with other angles when the relative wave number (kh) is in a range from 1.2 to 4.0. Differences only appear at the wave period of 8s corresponding to the kh of 0.5. Here, the Kd of the structure I_90°shows the smallest value of 0.41 while the I_135° has the highest Kd value of 0.7.

Previous studies by Rao et al. (2009); Yagci et al. (2014) showed an improvement in the wave damping capacity of inclined walls as well, however their results are not directly comparable due to different levels of inclination or submergence. For example, Yagci et al. (2014) performed a study on the effect of inclination angles, however they allowed for overtopping which is not the case in the presented study. Thus, their results might be underestimated. On the other hand, Rao et al. (2009) described the effect of the inclined directions in a similar way to this study, where opposite angles of the inclinations show comparable results, but under fully submerged conditions.

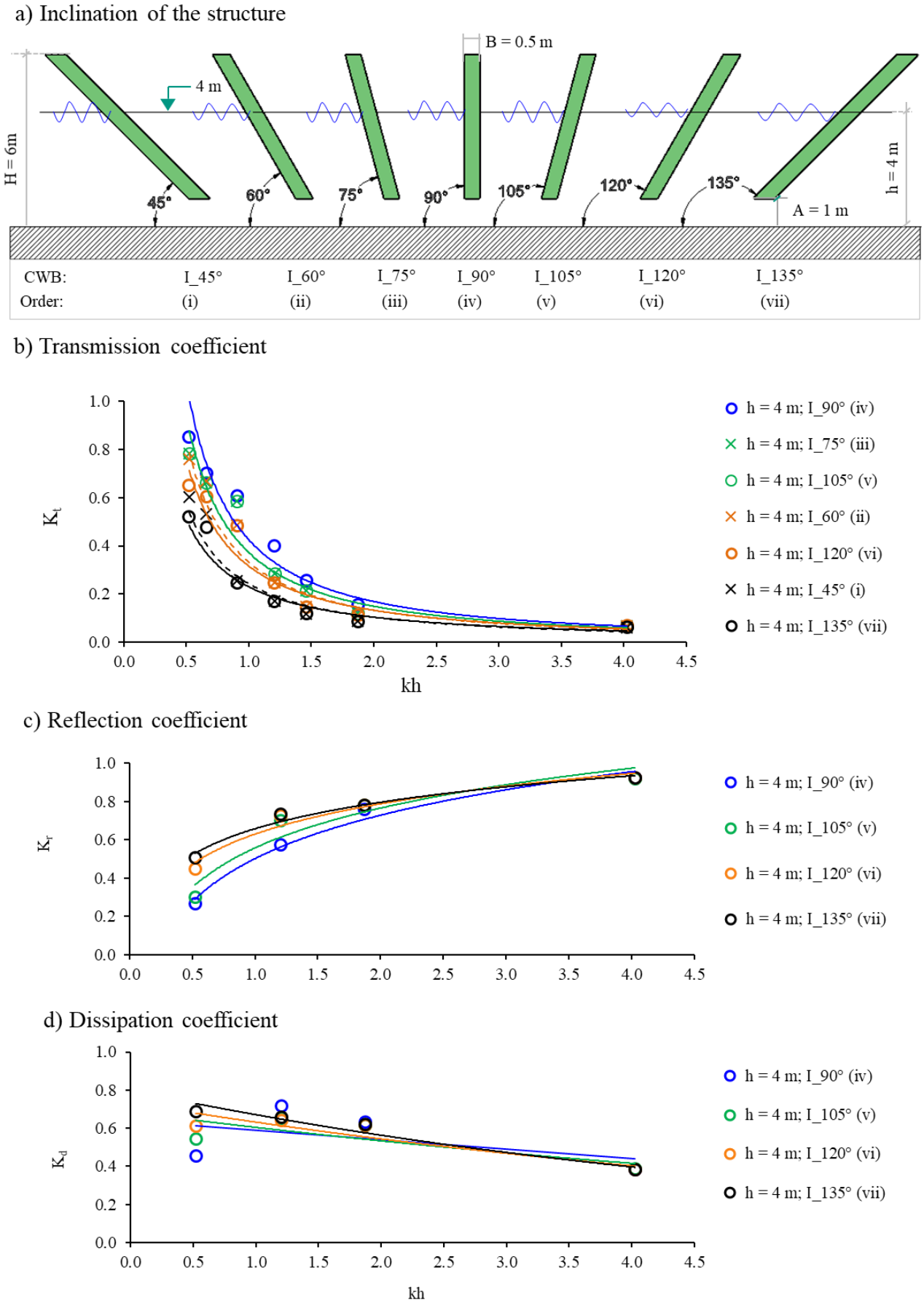

Figure 11: Effect of the inclination of the CWB variants on the wave characteristics.

4.2.2. Effect of the wall thickness

The effect of the structure thickness was examined for five CWB configurations in a range from a very thin wall of 0.05 m (B0.05) to a thick wall of 3 m (B3.0). All CWB variants have the same height of 6 m and a constant bottom gap of 1 m without supporting piers (see Figure 12a). Regarding the wave parameters, a range of wave periods of 2 s, 3 s, 3.5 s, 4 s, 5 s, 6 s, and 8 s were simulated with the wave heights of 0.4 m, 0.6 m, and 1.0 m, respectively, in 4 m water depth.

Wave transmission coefficients (K_t) are plotted versus the relative wave number (kh), the regression lines are power trendlines (Figure 12b). It indicates a clear trend of decreasing wave transmission towards a thicker structure. Particularly, the CWB configurations with a thickness between 0.05 m up to 1.0 m show only small differences regarding wave transmission coefficients as indicated in blue, orange, and green trendlines. The CWB configurations with the thicknesses of 2 m and 3 m show significantly higher rates of wave reduction illustrated in black and red trend lines. The transmission coefficient continuously decreases with increasing wave steepness from 0.018 (long wave period) to 0.11 (short wave period). Hence, the wave period of 8 seconds causes lowest efficiency in wave damping with Kt ranging from 0.6 to 0.9, while the highest wave damping efficiency occurs at the wave period of 2 seconds with Kt of 0.06.

Generally, thicker walls perform better than thinner ones in wave reduction. However, a thicker breakwater would need a larger amount of construction material, has a higher request for a stabilized foundation, and is therefore not favorable.

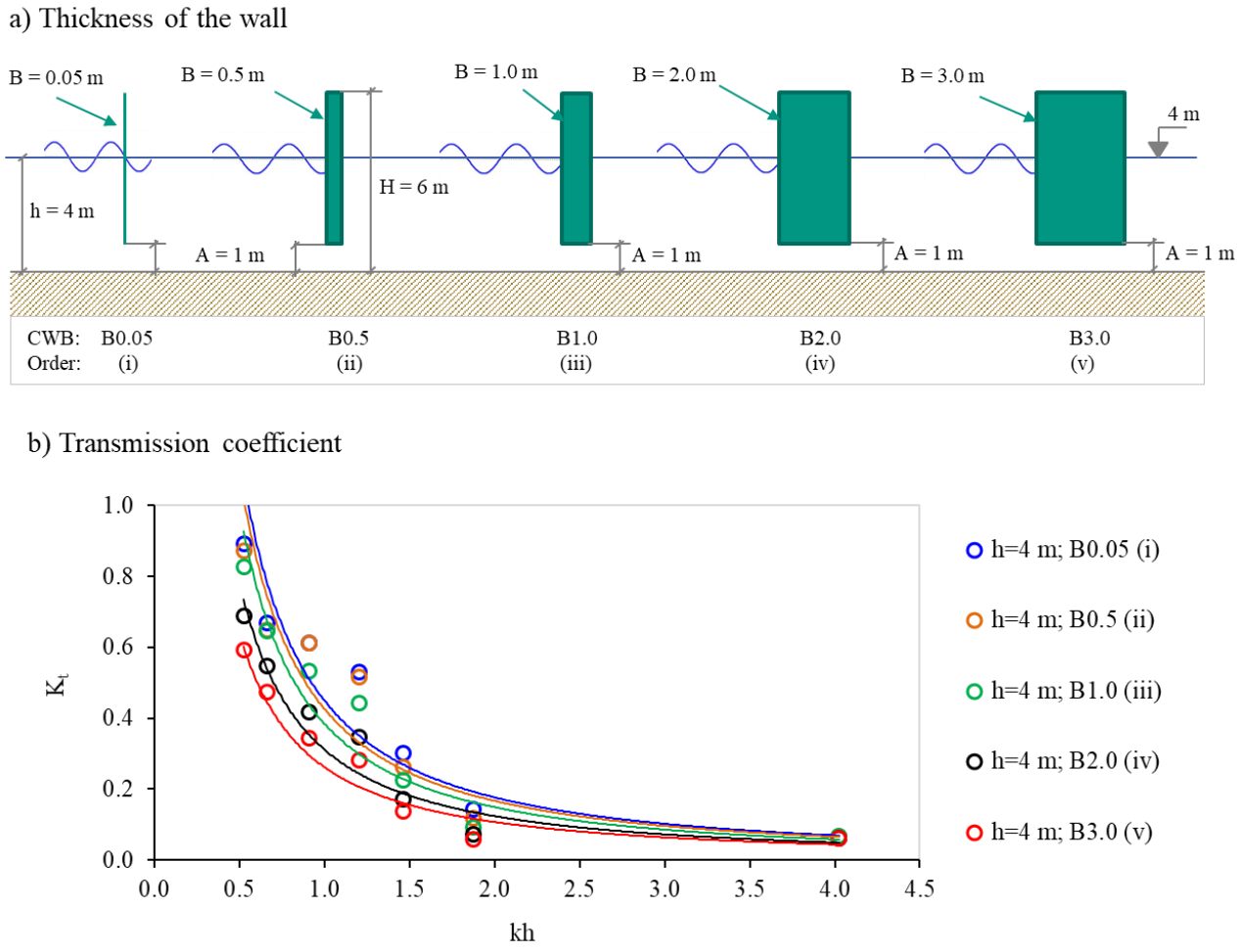

Figure 12: Effects of the thickness of the CWB variants on the wave characteristics.

4.2.3. Effects of the submerged draft and water depth

The effect of submerged draft was investigatedat different water depths ranging from 2 m to 5 m for the structure D1.0 as shown in Figure 13a. D1.0 has a constant draft of 1 m and is non-overtopping. The wave periods of 2 s, 4 s, 6 s, and 8 s corresponding to wave heights of 0.4 m, 0.6 m, and 1.0 m were simulated.

The wave transmission coefficients (Kt) are plotted versus the relative wave number (kh), exponential trendlines are applied as shownin Figure 13b. Overall, the effect of submerged draft and water depth shows a clear trend of reducing the wave transmission coefficient values from deep water (D/h = 0.2) to shallow water (D/h = 0.5). The structure D1 thereby performs better against short wave periods than long ones. Particularly, the Kt values range from 0.98 to 0.27 in the water depths of 4 m and 5 m following the increase in relative wave number (kh) from 0.5 to 5.0 (green and blue circles). In the shallow water of 2 m, the Kt values range from 0.8 to 0.25 according to the kh varying from 0.5 to 2.1.

The relative wave number (kh) has smaller values from 0.5 to 2.2 in shallow water of 2 m in comparison with deep water of 5 m with the kh ranging from 0.5 to 5.1 due to different wave lengths, although they have the same wave periods.

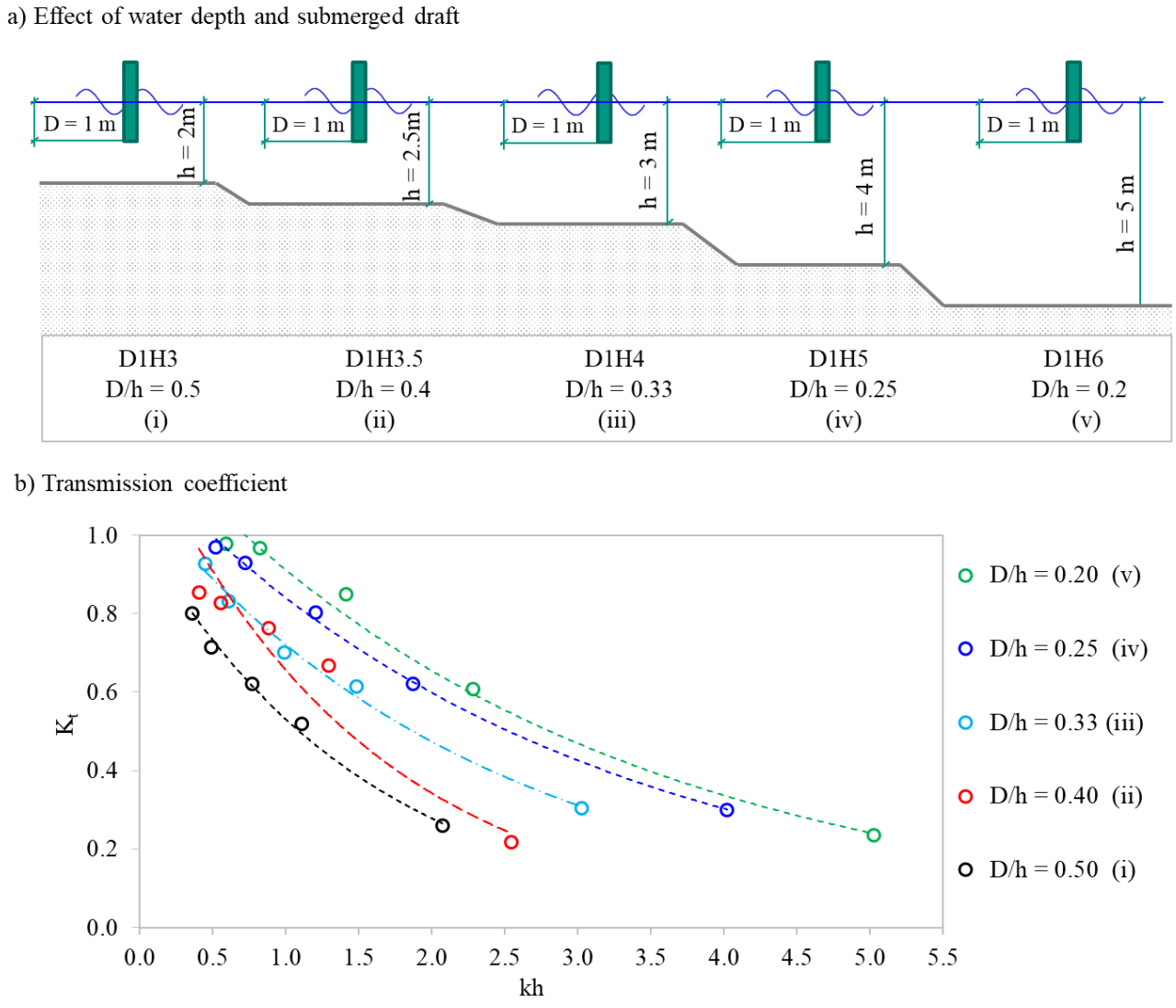

Figure 13: Effects of the submerged draft and water depth on the wave characteristics.

Our study on the effect of water depth and submerged draft contributes several results to previous research of CWB structures in this field. Particularly, the structure D1.0 (this study) placed in different water depths corresponding to D/h = 0.2 and D/h = 0.4 were selected to be compared with related research by Suh et al. (2005) and Ajiwibowo (2018). In their studies, Sue et al. (2005) examined three CWB configurations with multiple supporting piers, i.e., D1.44, D0.96,

D0.48 in a full-scale physical model as mentioned in Section 3.4, while Ajiwibowo (2018) performed a small-scale experiment for a single pier CWB in intermediate water depth. Exponential trendlines are applied in the comparison as seen in Figure 14. Interestingly, although the structures have different forms and compared in different water depths, the results of this study appropriately follow the distribution of K_t values by Suh et al. (2005) relating to the D/h rates verifying a clear trend with D/h values from 0.4 to 0.2. In contrast, the K_t results by Ajiwibowo (2018) show the smallest Kt value in the kh range from 0.8 – 1.8 for the D/h = 0.4 with a relative difference of 20 to 40%, which was explained by a scaling effect (Ajiwibowo 2018). The K_t values decrease when the ratio of D/h increases to 0.5 (this study) and 0.6 (Suh et al. 2005), which means that the structure has a small bottom gap. Hence, the effect of the bottom gaps was further investigated in the next Sub-section.

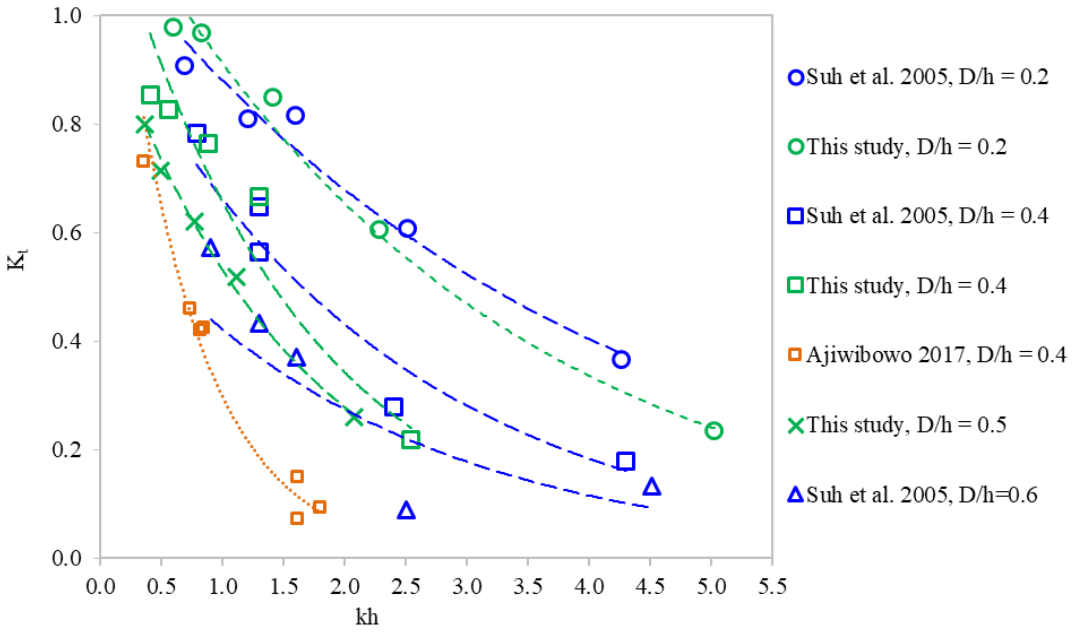

Figure 14: Effect of the submerged draft of the CWB configuration in comparison with related research.

4.2.4. Effects of the bottom gaps and supporting piers

The effect of bottom gaps and supporting piers was addressed in the intermediate water depth of 4 m for regular waves with a period of 4 s (the most dominant wave period in the MD), and wave heights varying from small wave to high wave (Hs = 0.2 m, 0.4 m, 0.6 m, 0.8 m, 1.0 m). Six CWB configurations were examined to evaluate the wave transmission through the structures under the condition of non-overtopping (Figure 15a). Table 4 presents the blockage rate of the CWB configurations. The blockage rate is defined as the ratio of the cross-sectional area of the CWB configurations with a closed wall.

Table 4. Blockage rate of CWB configurations

No.	Structure	a (m)	D (m)	W (m)	Pier amount	Pier surface area (m^2)	Pier spacing (m)	Cross-section area (m^2)	Blockage rate %
1	A3S-	3	1	3	0	0	-	3	25%
2	A3S0.2	3	1	3	4	6	0.2	9	75%
3	A2S-	2	2	3	0	0	-	6	50%
4	A2S0.2	2	2	3	4	4	0.2	10	83%
5	A1S-	1	3	3	0	0	-	9	75%
6	A1S0.2	1	3	3	4	2	0.2	11	92%
7	Closed wall	0	4	3	0	0	-	12	100%

The wave transmission coefficient is plotted versus the wave steepness (H_i/λ) and linear trendlines are used as shown in Figure 15b. It can be seen that a sole reduction of the bottom gap leads to a significant decrease in the wave transmission coefficient. Adding four piers (0.5 m x 0.5 m) with a pier spacing of 0.2 m significantly increases the wave damping efficiency of the structure. Besides, a higher wave steepness leads to a slight reduction in wave transmission. It can be concluded that the CWB variants with a reduced bottom gap perform slightly better against high waves than small waves.

Particularly, the structure A3S- with a bottom gap of 3m and a blockage rate of 25% has the highest wave transmission ranging from 0.86 to 0.98 (orange crosses). Here, the wave can transmit through the bottom gap while the upper part of the structure only causes a relatively small impact on the wave damping efficiency. However, when four supporting piers were added below, the A3S0.2 performed much better with a wave damping efficiency of around 20%, with K_t varying from 0.73 to 0.64 (orange circles). Interestingly, the K_t values of the CWB A3S0.2 (orange circles) are very similar to the wave transmission values caused by the structure A2S- (blue crosses), although they have different blockage rates of 75% and 50%, respectively. Similarly, with four piers added within the 2m gap, the A2S0.2 performed higher with a wave damping efficiency of 50%, and the K_t varies from 0.4 to 0.55 (blue circles). Besides, the K_t values of A2S0.2 are relatively similar to the wave transmission values caused by the structure A1S- (green crosses) with a small gap of 1 m. This indicates that a sole consideration of the blocked cross section, as suggested from different studies by Suh et al. (2018); Subekti et al. (2019); Rageh and Koraim (2010) is insufficient to predict the wave damping efficiency of a breakwater.

The structure A1S0.2 featuring the smallest gap with four supporting piers (blockage of 92%) mostly reduced the wave transmission through the structure with K_t values ranging from 0.2 to 0.22.

As a general trend, the reduction of the bottom gap and the implementation of supporting piers causes continuously decreasing transmission coefficients. Hence, these mentioned features could be used to control the transmission coefficient during the design process for a determined demand.

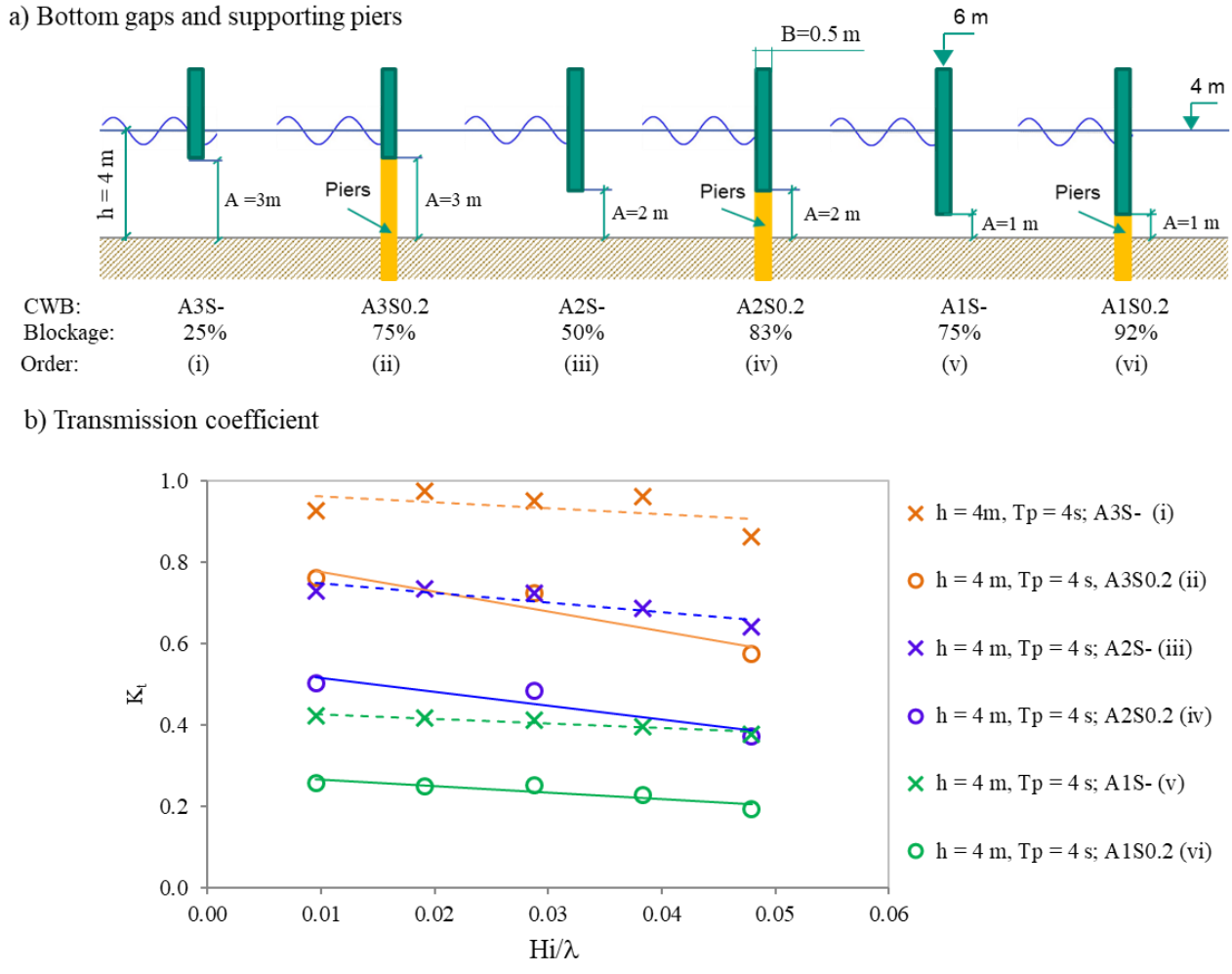

Figure 15: Effects of the bottom gaps and supporting piers on the wave characteristics.

4.2.4. Effects of structural heights and supporting piers

The effects of structural heights in combination with the effect of additional piers were investigated with a range of wave heights from 0.2 m to 1.0 m corresponding to a wave period of 4 s. Four CWB configurations were tested as shown in Figure 16a.

The wave transmission coefficient is plotted versus the wave steepness (H_i/λ) and linear trendlines are applied in Figure 16b. In the case of non-overtopping, a reduction of 20% in wave transmission can be recognized between the structures H6S- (no piers) and H6S0.2 (piers). The supporting piers, therefore, caused a high impact on wave damping efficiency. Particularly, the wave transmission Kt of H6S0.2 (green circles) varied from 0.2 to 0.22 in comparison with 0.4 to 0.42 in the case of no piers (green crosses), see Figure 16b.

In the case of overtopping, the Kt values of the structure H4S- without supporting piers varies in a stable range of 0.6 even when the wave steepness increases. The structure H4S0.2 with four supporting piers shows an increase in the wave transmission coefficient from 0.4 to 0.6 when the wave steepness increases due to increasing wave heights. This means that the effects of piers are more efficient in the case of small waves. However, the supporting piers do not impact in the case of high waves for the H4S- and H4S0.2 due to overtopping. It can be seen that K_t values of H4S- (blue crosses) and H4S0.2 (blue circles) are in a similar range of 0.6 when the wave steepness increases from 0.03 to 0.049.

In general, overtopping cases reduce the efficiency in wave damping of the CWB configurations. However, during storm surge conditions, the overtopping CWBs also have the advantage that unexpected high waves can easily overtop the structures and therefore prevent destruction of the breakwaters. Besides, an elimination of overtopping by design would request an uneconomic structural height and cause a higher demand for foundation stability.

a) Effect of supporting piers and structural heights

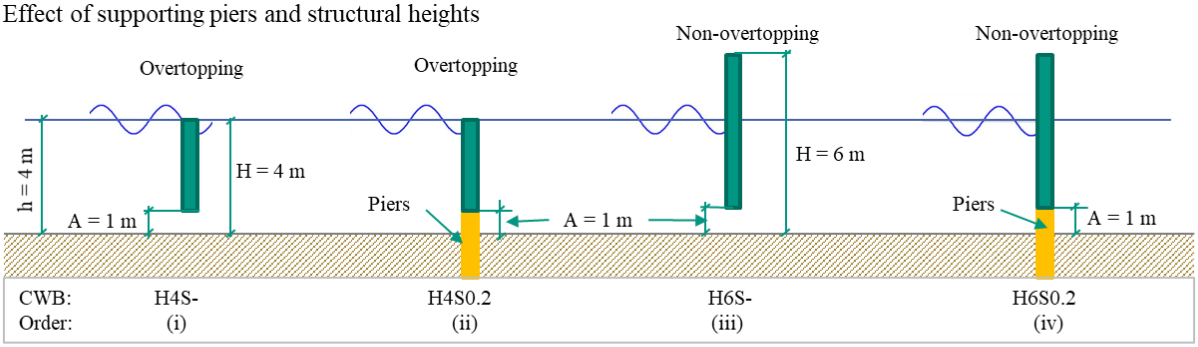

b) Transmission coefficient

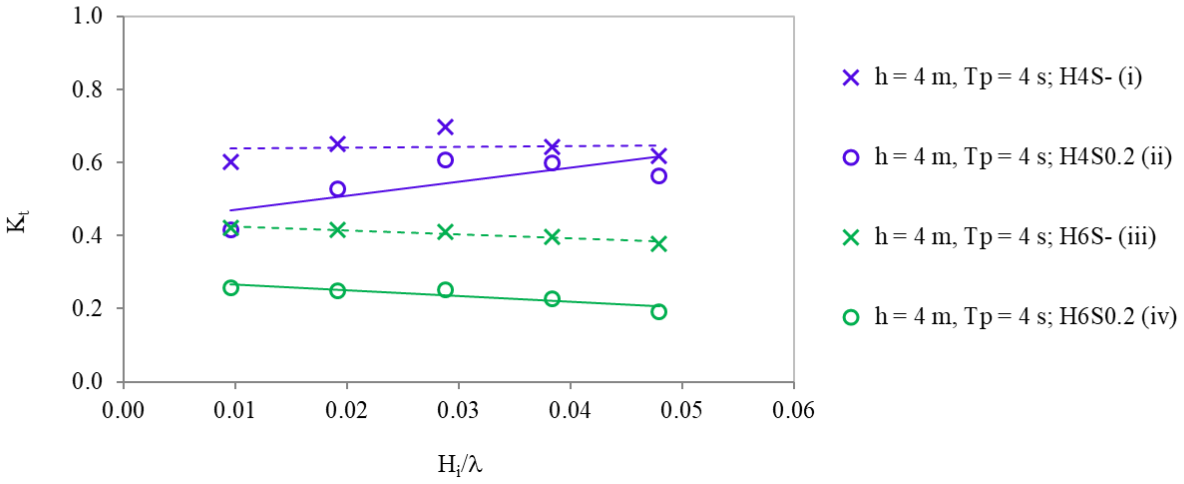

Figure 16: Effects of the supporting piers and structure heights on the wave characteristics.

4.2.4. Effects of tidal range and structural heights

The combined effect of overtopping with changing water depths was investigated against the background of tidal variations, which are present in many coastal areas. Therefore, the water depth was investigated in a range from 2 m to 5 m (Figure 17a), and wave heights were chosen between 0.2 m to 1.0 m corresponding to a wave period of 4 s. Two CWB configurations H4S0.2 and H6S0.2 corresponding to the heights of 4 m and 6 m were tested. Both variants featured a bottom gap of 1 m with supporting piers, a pier spacing of 0.2 m, and a wall thickness of 0.5 m.

The wave transmission coefficients (K_t) is plotted versus the wave steepness (H_i/λ) and linear trendlines are applied (Figure 17b). In the shallow water depths of 2 m and 3 m, the structure H4S0.2 acts as a non-overtopping breakwater, the wave transmission coefficient values range from 0.65 to 0.6 in the water depth of 2 m, and values are (from 0.4 to 0.38) in a water depth of 3 m, respectively (Figure 17b, blue and orange crosses). When the water depth reaches 4 m, the wave starts to overtop the breakwater H4S0.2. Hence, the transmission coefficient Kt starts increasing from 0.4 to a rather constant level of 0.6 (green crosses) following the increase in wave heights from 0.2 m to 1.0 m. The high wave can easily overtop the structure. The overall efficiency of H4S0.2 at 4m water depth thereby still ranges between the case for 2 m and 3 m. In contrast, the breakwater H6S0.2 still ensures the condition of non-overtopping at 4 m water depth. Therefore, it works more effectively with the Kt values ranging from 0.25 to 0.2 (green circles) following the increase in wave steepness from 0.01 to 0.049.

As expected, the fully (1m) submerged structure (H4S0.2) at a water depth of 5 m almost loses its wave damping efficiency with high transmission coefficient values close to 1 (black crosses). However, the K_t values of H6S0.2 (black circles) remain the same as investigated at 4 m water depth (green circles). Nevertheless, after reaching a wave height of 0.6 m corresponding to the wave steepness of 0.028, the wave starts to overtop the structure H6S0.2, which is indicated by increasing K_t values from 0.25 to 0.41 when the wave steepness increases from 0.028 and 0.046 (black circles) corresponding to the wave heights from 0.6 m to 1.0 m.

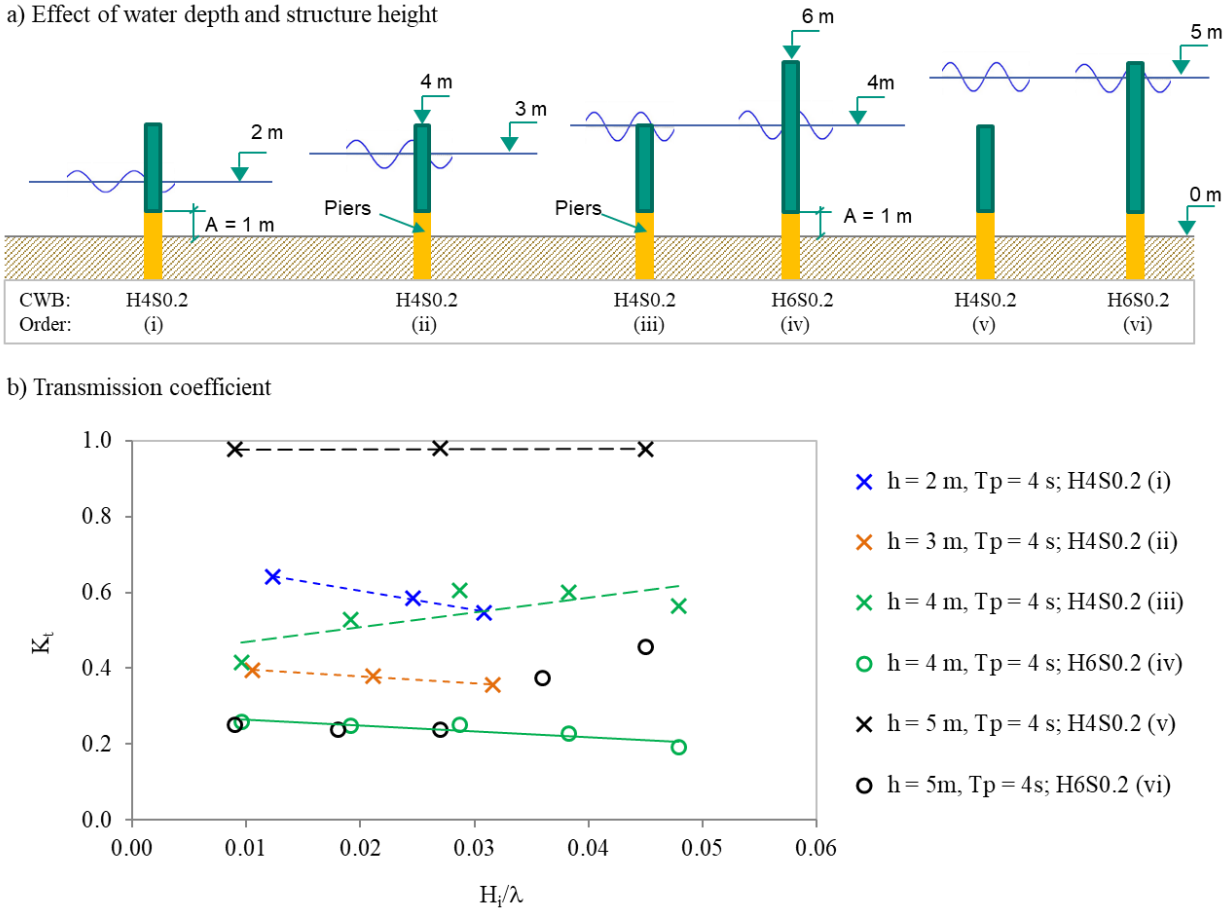

Figure 17: Effects of the water depth change and structure heights on the wave characteristics.

5 Limitation and orientation for future studies

Our study results are subject to limitations and uncertainties related to wave characteristics. Due to the restriction of our laboratory and the computational runtime in numerical modeling, we studied the wave-structure interaction under regular wave conditions. Although, regular wave analysis is a good preliminary design tool and as required design changes can be quickly assessed (Brekke et al. 2005), the transferability of the results for practical application under random wave conditions needs to be evaluated. We acknowledge these limitations and plan further investigations using random waves before implementing a pilot CWB in the field.

Up to now we evaluated several studies from other authors on the hydrodynamic performances of breakwaters under regular and random wave conditions. For instance, Yamamoto (1981) showed comparable results in wave transmission through a floating breakwater under random waves and regular waves. Besides, Neelamani et al. (2002) stated that the "⊥"-type breakwaters worked even more efficiently in random waves than in regular waves, while the trends in both approaches showed the same. Hence, it can be assumed that the wave transmission through CWBs in regular waves would have similar values/trends under random wave conditions.

6 Conclusions

This study provides a comprehensive investigation on the wave damping effects of Curtain Wall Breakwaters (CWBs) in terms of different geometric variations, wave characteristics, and tidal changes. The CFD platform was applied to examine the wave interactions through varying CWB configurations after showing a high agreement with experimental results. This study contributes several new results to the efficiency of CWBs regarding the curtain inclination, the effects of piers and bottom gaps, and the influence of tidal range and waves overtopping. The research findings lead to the following conclusions and recommendations:

- The different aspects of the CWB configurations mentioned above all show their impact on the wave transmission through the structures at different levels. In general, all structural variations showed the tendency to act more efficiently against short wave periods than long ones. While transmitting through the structures, short wave periods can interact more intensely on the breakwaters than longer ones, therefore leading to higher energy dissipation.
- The stronger the inclination from 90° up to 135°, the lower the wave transmission coefficient. Angles greater 135° might not be reasonable due to practical/construction issues and the amount of building materials. The direction of the inclination does not significantly affect the wave transmission, same angles in opposite directions, e.g. 45°vs 135° or 60° vs 120°, have comparable results.
- With an increase in the thickness of the wall, the wave transmission coefficient decreases. However, this trend is not linear. Wider structures might be unfavorable due to higher demands in construction materials and requirements on foundation stability.
- Regarding the water depth change due to the tidal range and structural heights, overtopping cases reduce the overall efficiency in wave reduction of the structures. In contrast, high structures that ensure non-overtopping conditions would perform much better regarding the wave reduction. However, a complete elimination of overtopping would request uneconomic structural heights.
- The smaller the bottom gap, the higher the wave energy dissipation of the structures. Adding supporting piers and a reduced bottom gap size leads to smaller wave transmission, where smaller gaps cause greater wave reduction than the big ones. Within a design process for CWBs, these aspects can be used to control the level of wave transmission when specific values are determined.
- Numerical modeling results show good agreement with physical tests that enhance the reliability of the numerical approach. On the other hand, this study focused on regular waves. Its transferability to more realistic conditions based on random waves needs to be assessed. Therefore, we recommend to further investigate wave damping of CWB structures under random wave conditions before building them in the field. Besides, important aspects such as scouring and foundation stability need to be studied alongside.

Based on the objective of developing an alternative breakwater to replace massive structures, and considering the conditions of soft soils, and gentle bathymetry gradients in the Mekong Delta, a curtain wall breakwater (CWB) concept might become a suitable solution in terms of foundation stability and less demand on construction materials to prevent the erosion process. By dissipating a certain part of the wave energy and allowing suspended sediment transport through the detached breakwaters for land reclamation and later for mangrove restoration, the coastal area may be protected in an ecological and sustainable way.

Acknowledgements

The work presented in this publication was performed within the framework of the ViWaT project which is sponsored by the German Federal Ministry for Education and Research BMBF (Grant number: 02WCL1474A). We offer our special thanks to Mr. Nguyen Thanh Tung (DARD Ca Mau), Mr. Le Xuan Tu (SIWRR) and Dr. Nguyet Minh (SIWRR) for kindly providing pictures of breakwaters and fruitful discussions within the project.

Author contributions (CRediT)

HTDV[1]: Conceptualization, Data curation, Formal analysis, Methodology, Software, Visualization, Writing – Original draft, and Writing – Review & Editing. MZ[2]: Conceptualization, Data curation, Methodology, Writing – Original draft, and Writing – Review & Editing. PO[3] and FS[4]: Conceptualization, Data curation, Methodology, Validation, Writing – Review & Editing, Project administration. FN[5]: Conceptualization, Methodology, Validation, Writing – Review & Editing, Project administration.

Acronyms and symbols

Acronyms	Description
BMBF	Federal Ministry of Education and Research, Germany
DARD Ca Mau	Department of Agricultural and Rural Development, Ca Mau province
IWG	Institute for Water and River Basin Management
KIT	Karlsruhe Institute of Technology, Germany
MD	Mekong Delta
SIWRR	Southern Institute of Water Resources Research, Vietnam
TRL	Theodor-Rehbock Laboratory
CWB	Curtain wall breakwater
CFD	Computational fluid dynamics
LES	Large eddy simulation model
RNG	Renormalized group model
WG	Wave gauge
Hs	Wave height (m)
Tp	Wave period (s)
h	Water depth (m)
λ	Wave length (m)
k	Wave number is defined as the number of wavelengths per unit distance; $k = 2\pi/\lambda$ (m^{-1})
kh	Relative wave number (-)

Acronyms	Description
Wave steepness	Ratio of wave height to wave length (Hs/λ) (-)
K_t	Wave transmission coefficient (-)
K_r	Wave reflection coefficient (-)
K_d	Wave energy dissipation coefficient (-)

References

Aau (2022): Aalborg University, Denmark. Wavelab program. Available online at https://www.hydrosoft.civil.aau.dk/wavelab.

Abdurrasheed, S.A.; Khamaruzaman, K.; Ebrahim, H.; Husna, T.; Aminuddin, A.; Muhammad, M. et al. (2019): Modelling of Flow Parameters through Subsurface Drainage Modules for Application in BIOECODS. In *Water* 11 (9), p. 1823. DOI: 10.3390/w11091823.

Acanal, L.; Loukogeorgaki, E.; Yagci, O.; Kirca, V. O.; Akgül, A. (2013): Performance of an inclined thin plate in wave attenuation. In *Journal of Coastal Research* 65, pp. 141–146. DOI: 10.2112/SI65-025.1.

Ajiwibowo, H. (2018): Physical Modeling For Measuring The Effectiveness Of Single Curtain Pile Foundation Breakwater In Intermediate Water Depth. In *GEOMATE* 14 (43). DOI: 10.21660/2018.43.43946.

Albers, T.; Stolzenwald, J. (2014): Coastal-engineering consultancy in the Ca Mua province. Integrated Coastal Management Programme (ICMP). Available online at www.giz.de/viet-nam.

Albers, T.; Dinh, C. S.; Schmitt, K. (2013): Shoreline management guidelines. Coastal protection in the lower Mekong Delta. With assistance of Deutsche Gesellschaft für Internationale Zusammenarbeit (GIZ) GmbH.

Alsaydalani, Majed O.; Saif, Mohammed A. N.; Helal, Medhat M. (2017): Hydrodynamic characteristics of three rows of vertical slotted wall breakwaters. In *J. Marine. Sci. Appl.* 16 (3), pp. 261–275. DOI: 10.1007/s11804-017-1427-5.

Anthony, Edward J.; Brunier, Guillaume; Besset, Manon; Goichot, Marc; Dussouillez, Philippe; van Nguyen, Lap (2015): Linking rapid erosion of the Mekong River delta to human activities. In *Scientific reports* 5, p. 14745. DOI: 10.1038/srep14745.

Atkins, Tom (2019): Design of a Partial Depth Wave Screen to Protect the Tawau Ferry Terminal, Malaysia. In Engineers Australia (Ed.): Proceedings of Australasian Coasts and Ports 2019 Conference. Hobart, 10-13 September 2019. Engineers Australia. Available online at https://search.informit.org/doi/10.3316/informit.796434794840168.

Bayon, A.; Valero, D.; García-Bartual, R.; Vallés-Morán, F. J.; López-Jiménez, P. A. (2016): Performance assessment of OpenFOAM and FLOW-3D in the numerical modeling of a low Reynolds number hydraulic jump. In *Environmental Modelling & Software* 80, pp. 322–335. DOI: 10.1016/j.envsoft.2016.02.018.

Behnam, S., Mehboudi, A. (2016): Numerical modeling of local scour at the junction of open channels in Flow3D numerical model Vol. 2, No. 9, September, 2016.

Besset, Manon; Gratiot, Nicolas; Anthony, Edward J.; Bouchette, Frédéric; Goichot, Marc; Marchesiello, Patrick (2019): Mangroves and shoreline erosion in the Mekong River delta, Viet Nam. In *Estuarine, Coastal and Shelf Science* 226, p. 106263. DOI: 10.1016/j.ecss.2019.106263.

Brekke, J; Chakrabarti, S. (2005): Chapter 9 – Drilling and production risers. In Handbook of Offshore Engineering, pages 709-859. DOI: 10.1016/B978-0-08-044381-2.50016-3.

Bloxam, Martin; Maxted, Gordon; Murray, John (2003): Wave Energy Dissipating Wharf: Raffles Marina Breakwater, Singapore. In : In: Kench, Paul S.; Hume, Terry M. Coasts & Ports 2003 Australasian Conference : Proceedings of the 16th Australasian Coastal and Ocean Engineering Conference, the 9th Australasian Port and Harbour Conference and the Annual New Zealand Coastal Society Conference. Barton, A.C.T.: Institution of Engineers, Australia, 2003: [796]-[805]. Available online at https://search.informit.org/doi/10.3316/informit.256180017252878.

Cho, I. H.; Kim, M. H. (2008): Wave absorbing system using inclined perforated plates. In *Journal of Fluid Mechanics* 608, pp. 1–20. DOI: 10.1017/S0022112008001845.

Chu, V. C.; Brown, S.; To, H. H.; Hockings, M. (2015): Using Melaleuca fences as soft coastal engineering for mangrove restoration in Kien Giang, Vietnam. In *Ecological Engineering* 81, pp. 256–265. DOI: 10.1016/j.ecoleng.2015.04.031.

Dao, H. T.; Hofland, B.; Suzuki, T.; Stive, M.J.F.; Mai, T.; Le, T. X. (2021): Numerical and small-scale physical modelling of wave transmission by wooden fences. Journal of Coastal and Hydraulic Structures, Vol. 1 (2021): Single articles. DOI: 10.48438/JCHS.2021.0004.

DARD Camau (2021): Evaluation of existing coastal protection structures in Camau province. Minutes of Meeting.

Dung, V. T.; Dang, T. D.; Galelli, S.; Hossain, F. (2021): Satellite observations reveal thirteen years of reservoir filling strategies, operating rules, and hydrological alterations in the Upper Mekong River Basin. DOI: 10.5194/hess-2021-360.

Elsheikh, Ahmed K.; Mostafa, Yasser E.; Mohamed, Mostafa M. (2022): A comparative study between some different types of permeable breakwaters according to wave energy dissipation. In *Ain Shams Engineering Journal* 13 (4), p. 101646. DOI: 10.1016/j.asej.2021.11.015.

Fard, A.R.T. (2020): Influence of Vegetation on Shear Stress and Flow Rate in Open Channel using Flow3D. In *CERJ* 9 (5). DOI: 10.19080/CERJ.2020.09.555774.

Flow Science (2008): FLOW-3D User Manual V9.3.

Franco, Leopoldo (1994): Vertical breakwaters: the Italian experience. In *Coastal Engineering* 22 (1-2), pp. 31–55. DOI: 10.1016/0378-3839(94)90047-7.

Frese, Marianne; Bleck, Matthias; Schöner, Michael (2012): Tauchwände als Wellenbrecher. In *Bautechnik* 89 (5), pp. 333–337. DOI: 10.1002/bate.201201548.

Fuentes-Pérez, J. F.; Quaresma, A. L.; Pinheiro, A.; Sanz-Ronda, F. J. (2022): OpenFOAM vs FLOW-3D: A comparative study of vertical slot fishway modelling. In *Ecological Engineering* 174, p. 106446. DOI: 10.1016/j.ecoleng.2021.106446.

Gems, B.; Mazzorana, B.; Hofer, T.; Sturm, M.; Gabl, R.; Aufleger, M. (2016): 3D-hydrodynamic modelling of flood impacts on a building and indoor flooding processes. DOI: 10.5194/nhess-2015-326.

GIZ (2016): Integrated coastal protection and mangrove belt rehabilitation in the Mekong Delta. Pre-feasibility study for investments in coastal protection along 480 kilometers in the Mekong Delta: Deutsche Gesellschaft für Internationale Zusammenarbeit (GIZ) GmbH.

Hirt, C.W.; Nichols, B.D. (1981): Volume of fluid (VOF) method for the dynamics of free boundaries. In Journal of Computational Physics 39, page 201-225. DOI: 10.1016/0021-9991(81)90145-5.

Jordan, C.; Tiede, J.; Lojek, O.; Visscher, J.; Apel, H.; Nguyen, H. Q. et al. (2019): Sand mining in the Mekong Delta revisited - current scales of local sediment deficits. In Scientific reports 9 (1), p. 17823. DOI: 10.1038/s41598-019-53804-z.

Goldberg, Liza; Lagomasino, David; Thomas, Nathan; Fatoyinbo, Temilola (2020): Global declines in human-driven mangrove loss. In *Global change biology* 26 (10), pp. 5844–5855. DOI: 10.1111/gcb.15275.

Gruel, C.; Park, E.; Ho, L.; Kantoush, S.; Feng, L.; Doan, V. B.; Switzer, A. (2021): New systemically measured sand mining budget for the Mekong Delta reveals rising trends and significant volume underestimations. DOI: 10.31223/X5H61H.H. A. Ariyarathne (2007): Efficiency of perforated breakwater and associated energy dissipation.

Hamilton, Stuart E.; Casey, Daniel (2016): Creation of a high spatio-temporal resolution global database of continuous mangrove forest cover for the 21st century (CGMFC-21). In *Global Ecol. Biogeogr.* 25 (6), pp. 729–738. DOI: 10.1111/geb.12449.

Hecht, J. S.; Guillaume, L.; Mauricio, E. A.; Thanh, D. D.; Thanapon, P. (2019): Hydropower dams of the Mekong River basin: A review of their hydrological impacts. In *Journal of Hydrology* 568, pp. 285–300. DOI: 10.1016/j.jhydrol.2018.10.045.

Hooijer, A.; Vernimmen, R. (2021): Global LiDAR land elevation data reveal greatest sea-level rise vulnerability in the tropics. In *Nature communications* 12 (1), p. 3592. DOI: 10.1038/s41467-021-23810-9.

Hu, Hui; Zhang, Jianfeng; Li, Tao (2018): Dam-Break Flows: Comparison between Flow-3D, MIKE 3 FM, and Analytical Solutions with Experimental Data. In *Applied Sciences* 8 (12), p. 2456. DOI: 10.3390/app8122456.

Isaacson, Michael; Baldwin, John; Premasiri, Sundarlingam; Yang, Gang (1999): Wave interactions with double slotted barriers. In *Applied Ocean Research* 21 (2), pp. 81–91. DOI: 10.1016/S0141-1187(98)00039-X.

Isaacson, Michael; Premasiri, Sundarlingam; Yang, Gang (1998): Wave Interactions with Vertical Slotted Barrier. In *J. Waterway, Port, Coastal, Ocean Eng.* 124 (3), pp. 118–126. DOI: 10.1061/(ASCE)0733-950X(1998)124:3(118).

Ji, Chang-Hwan; Suh, Kyung-Duck (2010): Wave interactions with multiple-row curtainwall-pile breakwaters. In *Coastal Engineering* 57 (5), pp. 500–512. DOI: 10.1016/j.coastaleng.2009.12.008.

Kim, d.W.; Lexmond, B. R.; Stouthamer, E.; Neussner, O.; Dörr, N.; Schenk, A.; Minderhoud, P.S.J. (2021): Identifying Causes of Urban Differential Subsidence in the Vietnamese Mekong Delta by Combining InSAR and Field Observations. In *Remote Sensing* 13 (2), p. 189. DOI: 10.3390/rs13020189.

Koraim, A. S. (2014): Hydraulic characteristics of pile-supported L-shaped bars used as a screen breakwater. In *Ocean Engineering* 83, pp. 36–51. DOI: 10.1016/j.oceaneng.2014.03.016.

Koraim, A. S.; Heikal, E. M.; Rageh, O. S. (2011): Hydrodynamic characteristics of double permeable breakwater under regular waves. In *Marine Structures* 24 (4), pp. 503–527. DOI: 10.1016/j.marstruc.2011.06.004.

Koraim, A. S.; Iskander, M. M.; Elsayed, W. R. (2014): Hydrodynamic performance of double rows of piles suspending horizontal c shaped bars. In *Coastal Engineering* 84, pp. 81–96. DOI: 10.1016/j.coastaleng.2013.11.006.

Kosaj, R.; Alboresha, R. S.; Sulaiman, S. O. (2022): Comparison Between Numerical Flow3d Software and Laboratory Data, For Sediment Incipient Motion. In *IOP Conf. Ser.: Earth Environ. Sci.* 961 (1), p. 12031. DOI: 10.1088/1755-1315/961/1/012031.

Laju, Kottalil; Sundar, Vallam; Sundaravadivelu, Ranganathan (2011): Hydrodynamic characteristics of pile supported skirt breakwater models. In *Applied Ocean Research* 33 (1), pp. 12–22. DOI: 10.1016/j.apor.2010.12.004.

Le, X. T.; Le, M. H.; Tran, B. H.; v.d. Do; Vu, H.T.D.; Wright, D. et al. (2021): Wave energy dissipation through a hollow triangle breakwater on the coastal Mekong Delta. In *Ocean Engineering* 245, p. 110419. DOI: 10.1016/j.oceaneng.2021.110419.

Le, X. T.; Tran, B. H.; Le, M. H.; v.d. Do; Nguyet, M. N.; Wright, P. D. et al. (2020): Hydraulic performance and wave transmission through pile-rock breakwaters. In *Ocean Engineering* 218, p. 108229. DOI: 10.1016/j.oceaneng.2020.108229.

Le, X. T.; Vo, Q. T.; Johan, R.; Song, P. V.; Tran, A. D.; Thanh, D. D.; Dano, R. (2019): Sediment transport and morphodynamical modeling on the estuaries and coastal zone of the Vietnamese Mekong Delta. In *Continental Shelf Research* 186, pp. 64–76. DOI: 10.1016/j.csr.2019.07.015.

Leatherman, Stephen P.; Zhang, Keqi; Douglas, Bruce C. (2000): Sea level rise shown to drive coastal erosion. In *Eos Trans. AGU* 81 (6), p. 55. DOI: 10.1029/00EO00034.

Lee, J. Y.; Kweon, H. M.; Lee, J. L. (2009): Wave Scattering and Beach Morphodynamics behind a Permeable Curtain Wall-Pile Breakwater of Finite Length. In *Journal of Coastal Research*, pp. 995–999. Available online at www.jstor.org/stable/25737936.

Liu, Yong; Li, Yu-cheng (2011): Wave interaction with a wave absorbing double curtain-wall breakwater. In *Ocean Engineering* 38 (10), pp. 1237–1245. DOI: 10.1016/j.oceaneng.2011.05.009.

Luom, T. T.; Phong, N. T.; Anh, N. T.; Tung, N. T.; Le, T. X.; Duong, T. A. (2021): Using Fine-Grained Sediment and Wave Attenuation as a New Measure for Evaluating the Efficacy of Offshore Breakwaters in Stabilizing an Eroded Muddy Coast: Insights from Ca Mau, the Mekong Delta of Vietnam. In *Sustainability* 13 (9), p. 4798. DOI: 10.3390/su13094798.

Marchesiello, Patrick; Nguyen, Nguyet Minh; Gratiot, Nicolas; Loisel, Hubert; Anthony, Edward J.; Dinh, Cong San et al. (2019): Erosion of the coastal Mekong delta: Assessing natural against man induced processes. In *Continental Shelf Research* 181, pp. 72–89. DOI: 10.1016/j.csr.2019.05.004.

Masard, E.P.D.; Funke, E. R. (1980): The Measurement of Incident and Reflected Spectra Using a Least squares Method. Incicent and reflected spectra.

Masselink, G.; Russell, P.; Rennie, A.; Brooks, S.; Spencer, T. (2020): Impacts of climate change on coastal geomorphology and coastal erosion relevant to the coastal and marine environment around the UK.

Minderhoud, P. S. J.; Coumou, L.; Erban, L. E.; Middelkoop, H.; Stouthamer, E.; Addink, E. A. (2018): The relation between land use and subsidence in the Vietnamese Mekong delta. In *The Science of the total environment* 634, pp. 715–726. DOI: 10.1016/j.scitotenv.2018.03.372.

Minderhoud, P. S. J.; Coumou, L.; Erkens, G.; Middelkoop, H.; Stouthamer, E. (2019): Mekong delta much lower than previously assumed in sea-level rise impact assessments. In *Nature communications* 10 (1), p. 3847. DOI: 10.1038/s41467-019-11602-1.

Minh, N. N.; Dinh, C. S.; Duong, D. V.; Nestmann, F.; Zemann, M.; Vu, H.T.D.; Dan, T. C. (2020): Evaluating the effectiveness of existing coastal protection measures in Mekong Delta, pp. 1419–1429.

Musall and Oberle (2014): Numerical Simulation of Flow Characteristics in Vertical Slot Fishways Proceedings 10th Intl. Symposium on EcoHydraulics 2014, Trondheim, Norway.

Neelamani, S.; Rajendran, R. (2002): Wave interaction with '⊥'-type breakwaters. In Ocean Engineering 29, Issue 5, pages 561-589. DOI: 10.1016/S0029-8018(01)00030-0.

Nejadkazem, O.; Mostafa Gharabaghi, A. R. (2013): The permeability parameter of curtain-wall breakwaters. In *Proceedings of IMarEST - Part A - Journal of Marine Engineering and Technology* 12. DOI: 10.1080/20464177.2013.11020274.

Nguyen, T. B.; van Thuy, T.; Nguyen, A. M.; Nguyen, N. M.; Nguyen, H. T. (2021): Drivers of agricultural transformation in the coastal areas of the Vietnamese Mekong delta. In *Environmental Science & Policy* 122, pp. 49–58. DOI: 10.1016/j.envsci.2021.04.010.

Nguyen, C.P.; Vu, H.T.D.; Vu, H.L.; Schenk, A.; Oberle, P.; Tran, D.D. (2022): Datasets of land use change and flood dynamics in the vietnamese mekong delta. In Data in Brief 22, 108268. DOI: 10.1016/j.dib.2022.108268.

Nugroho, D.; Yovita, I. V.; Sufyan, A.; Mahabror, D.; Rudhy, A. (2021): The application of semi-submersible geotextile tubes for coastal protection in Pamekasan, Madura. In *IOP Conf. Ser.: Earth Environ. Sci.* 860 (1), p. 12100. DOI: 10.1088/1755-1315/860/1/012100.

Park, E.; Loc, H. H.; Binh, D. V.; Kantoush, S. (2021): The worst 2020 saline water intrusion disaster of the past century in the Mekong Delta: Impacts, causes, and management implications. In *Ambio*. DOI: 10.1007/s13280-021-01577-z.

Parsons, N. F.; Martin, P. A. (1992): Scattering of water waves by submerged plates using hypersingular integral equations. In *Applied Ocean Research* 14 (5), pp. 313–321. DOI: 10.1016/0141-1187(92)90035-I.

Phan, Linh K.; van Thiel de Vries, Jaap S.M.; Stive, Marcel J.F. (2015): Coastal Mangrove Squeeze in the Mekong Delta. In *Journal of Coastal Research* 300, pp. 233–243. DOI: 10.2112/JCOASTRES-D-14-00049.1.

Pörtner, H., O.; Roberts, D. C.; Poloczanska, E. S.; Mintenbeck, K.; Tignor M.; Alegría, A.; Craig M.; Langsdorf, S.; Löschke, S.; Möller, V.; Okem, A. (2022): Intergovernmental Panel on Climate Change: Climate Change 2022 - Impacts, Adaptation and Vulnerability. Summary for policymakers. ISBN 978-92-9169-159-3.

Rageh, O. S.; Koraim, A. S. (2010): Hydraulic performance of vertical walls with horizontal slots used as breakwater. In *Coastal Engineering* 57 (8), pp. 745–756. DOI: 10.1016/j.coastaleng.2010.03.005.

Rao, S.; Kiran G. Shirlal; Roobin V. Varghese; Kumaresan Govindaraja (2009): Physical model studies on wave transmission of a submerged inclined plate breakwater. In *Ocean Engineering* 36, pp. 1199–1207.

REEF3D (2022): Open-source Hydrodynamic. Available online at https://reef3d.wordpress.com/.

Shin, E.C.l; Kim, S. H.; Hakam, A.; Istijono, B. (2019): Erosion problems of shore line and counter measurement by various geomaterials. In *MATEC Web Conf.* 265, p. 1010. DOI: 10.1051/matecconf/201926501010.

Song, P. V.; Vu, H.T.D. (2012): Stilling basin design in downstream of Thu Bo barrier by numerical and physical models. In *Science of Water Resources Engineering and Environment* Nr.37 (06/2012).

Subekti; Darsono; Yowono (2019): Wave Transmission Through Curtainwall Pile Breakwater (CPB) (Volume: 10). In *International Journal of Civil Engineering and Technology (IJCIET)* (Issue: 6), Pages: 389-398.

Subekti, Subekti; Shulhany, Ahmad (2021): Transmission and reflection of waves on curtain wall breakwater. In *tjst* 17 (1), p. 100. DOI: 10.36055/tjst.v17i1.11026.

Suh, K. D.; Shin, S.; Cox, D. T. (2005): Hydrodynamic Characteristics of Curtain-Wall-Pile Breakwaters. Available online at https://www.researchgate.net/publication/267990906_Hydrodynamic_characteristics_of_curtain-wall-pile_breakwaters.

Suh, Kyung-Duck; Ji, Chang-Hwan; Kim, Bum Hyoung (2011): Closed-form solutions for wave reflection and transmission by vertical slotted barrier. In *Coastal Engineering* 58 (12), pp. 1089–1096. DOI: 10.1016/j.coastaleng.2011.06.001.

Suh, Kyung-Duck; Jung, Hoo Young; Pyun, Chong Kun (2007): Wave reflection and transmission by curtainwall–pile breakwaters using circular piles. In *Ocean Engineering* 34 (14-15), pp. 2100–2106. DOI: 10.1016/j.oceaneng.2007.02.007.

Suh, Kyung-Duck; Shin, Sungwon; Cox, Daniel T. (2006): Hydrodynamic Characteristics of Pile-Supported Vertical Wall Breakwaters. In *J. Waterway, Port, Coastal, Ocean Eng.* 132 (2), pp. 83–96. DOI: 10.1061/(ASCE)0733-950X(2006)132:2(83).

Tran, D. D.; Vu, H.T.D.; Van, T. C.; Oberle, P.; Hinz, S.; Nestmann, F. (2021): Evaluating the Impacts of Rice-Based Protection Dykes on Floodwater Dynamics in the Vietnamese Mekong Delta Using Geographical Impact Factor (GIF). In *Water* 13 (9), p. 1144. DOI: 10.3390/w13091144.

Tuan, T. Q.; Luan, M. T. (2020): Monsoon wave transmission at bamboo fences protecting mangroves in the lower mekong delta. In *Applied Ocean Research* 101, p. 102259. DOI: 10.1016/j.apor.2020.102259.

United Nations (2017). Factsheet: People and Oceans. The Ocean Conference, United Nations, New York, 5-9 June 2017.

Ursell, F. (1947): The effect of a fixed vertical barrier on surface waves in deep water. In *Mathematical Proceedings of the Cambridge Philosophical Society* 43 (3), pp. 374–382. DOI: 10.1017/S0305004100023604.

Vu, H.T.D; Nestmann, F.; Trinh, C.V.; Oberle, P.; Hinz, S.; Geiger, H. (2016): Geographical impact of dyke measurement for land use on flood water in the Mekong Delta. Available online at https://www.researchgate.net/publication/303370408.

Vu, H.T.D.; Trinh, C.V.; Nestmann, F.; Oberle, P.; Nam, N. T. (2014): Land use based flood hazard analysis for the Mekong Delta. In *Proceedings of the 19th IAHR-APD Congress 2014, Hanoi, Vietnam*. DOI: 10.13140/2.1.5153.9842.

Vu, H.T.D. (2019): Land Use Based Flood Hazard Analysis for the Mekong Delta. Doctoral dissertation, Karlsruhe, Germany. Karlsruhe Institute of Technology. Available online at https://doi.org/10.5445/IR/1000089862.

Vu, H.T.D.; Tran, D. D.; Schenk, A.; Nguyen, C.P, Vu, H.L.; Oberle, P.; Van, T. C.; Nestmann, F. (2022): Land use change in the Vietnamese Mekong Delta: New evidence from remote sensing. In *The Science of the total environment*, p. 151918. DOI: 10.1016/j.scitotenv.2021.151918.

Yagci, Oral; Kirca, V. OzgurS.; Acanal, Lami (2014): Wave attenuation and flow kinematics of an inclined thin plate acting as an alternative coastal protection structure. In *Applied Ocean Research* 48, pp. 214–226. DOI: 10.1016/j.apor.2014.09.003.

Yamamoto, T. (1981): Moored floating breakwater response to regular and irregular waves. In Applied Ocean Research, Volume 3, Issue 1, Pages 27-36. DOI: 10.1016/0141-1187(81)90082-1.

Zhu, Y.; Li, Yu; T. A.; Zhang, J. (2015): Numerical Modeling of Wave Interaction with Double Curtain-wall Breakwater. In Procedia Engineering 116, pp. 1009–1018. DOI: 10.1016/j.proeng.2015.08.393.

Appendix

Figure A1: Several existing coastal protection measures in the Mekong Delta (Source: images were collected from GIZ (2016); SIWRR; DARD Camau; and KIT).

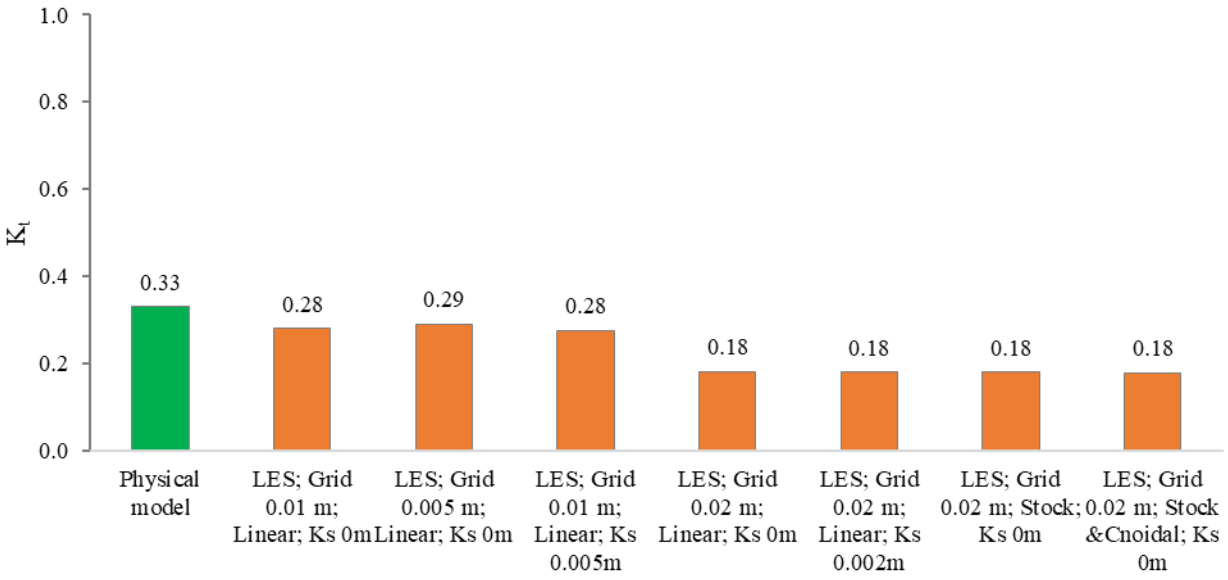

Figure A2: Validation of wave transmission through the structure A0.1S0.02.

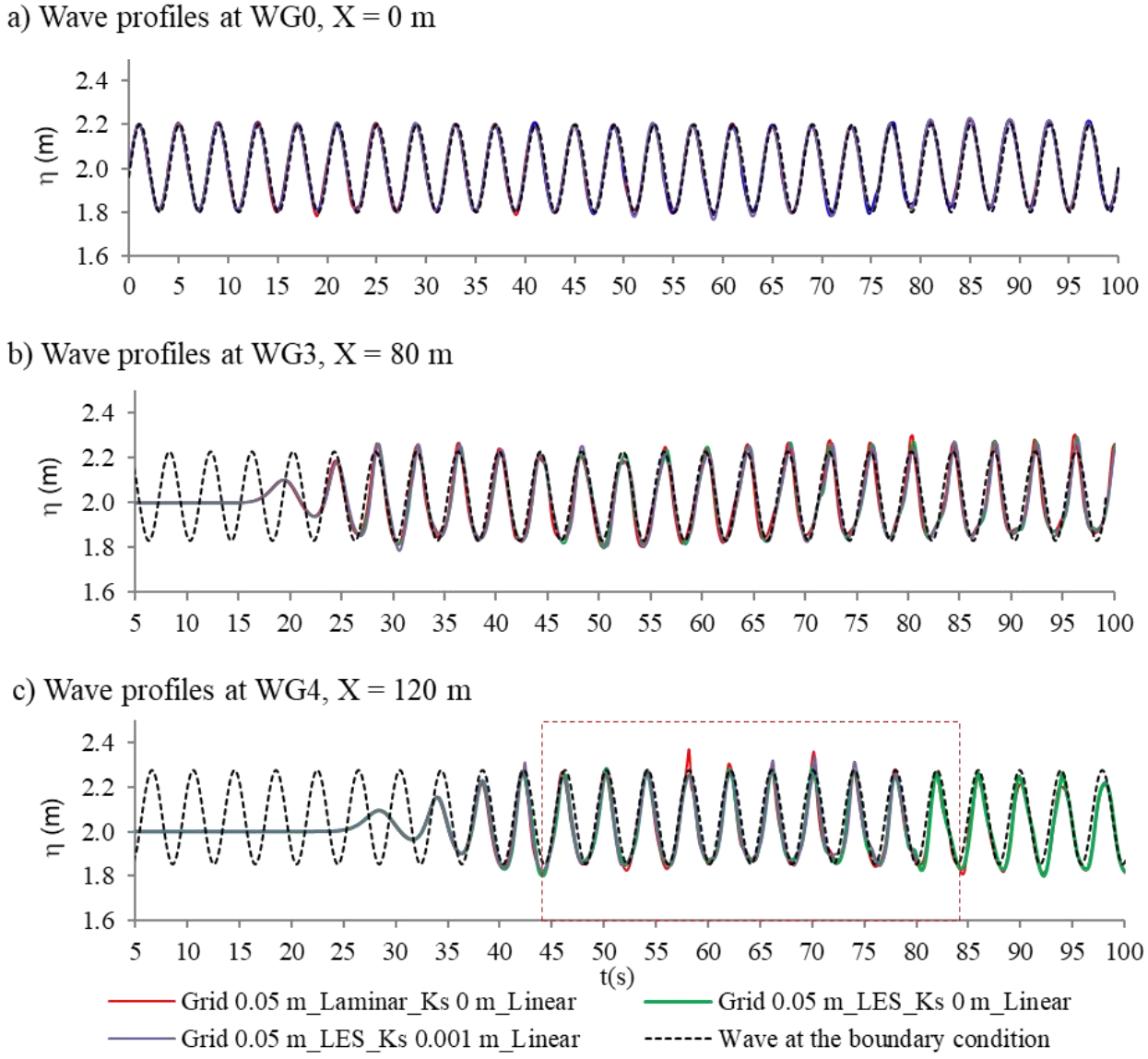

Figure A3: Wave profiles along the blank flume at WG0, WG3, WG4 in the numerical model.

Table A1: Sensitivity analysis of simulated results at WG4 for the case of no structures.

No.	Input parameters				Boundary conditions			Simulated results at WG4	
	Turbulence options	Wave	Ks (m)	Grid size (m)	h (m)	Hs (m)	Tp (s)	Hs (m)	Tp (s)
1	LES model	Linear	0.000	0.20	2.0	0.4	4.0	0.409	4.02
2	LES model	Linear	0.000	0.10	2.0	0.4	4.0	0.411	3.96
3	LES model	Linear	0.000	0.05	2.0	0.4	4.0	0.406	4.00
4	LES model	Linear	0.000	0.02	2.0	0.4	4.0	0.400	4.01
5	Laminar	Linear	0.000	0.05	2.0	0.4	4.0	0.414	4.00
6	k-e model	Linear	0.000	0.05	2.0	0.4	4.0	0.407	3.99
7	k-ω model	Linear	0.000	0.05	2.0	0.4	4.0	0.417	4.01
8	RNG model	Linear	0.000	0.05	2.0	0.4	4.0	0.408	4.00
9	LES model	Stokes	0.000	0.05	2.0	0.4	4.0	0.424	3.99
10	LES model	Stokes & Cnoidal	0.000	0.05	2.0	0.4	4.0	0.413	4.01
11	LES model	Linear	0.001	0.05	2.0	0.4	4.0	0.414	4.01
12	LES model	Linear	0.010	0.05	2.0	0.4	4.0	0.410	3.99
13	LES model	Linear	0.025	0.05	2.0	0.4	4.0	0.411	3.99